

The Pennsylvania State University
The Graduate School

**A DYNAMIC LINK BUDGET FOR SATELLITE COMMUNICATION
BASED ON THE CYCLIC NATURE OF GALACTIC NOISE**

A Thesis in
Electrical Engineering
by
Terele Parker

© 2022 Terele Parker

Submitted in Partial Fulfillment
of the Requirements
for the Degree of

Master of Science

August 2022

The thesis of Terele Parker was reviewed and approved by the following:

Julio Urbina
Associate Professor of Electrical Engineering
Thesis Co-Advisor

James Breakall
Professor of Electrical Engineering
Thesis Co-Advisor

Erik H. Lenzing
Deputy Department Head of CINO
ARL Advisor

Kultegin Aydin
Professor of Electrical Engineering
Head of the Electrical Engineering Department
at Penn State

ABSTRACT

This thesis serves to address the commonly over compensation of a natural occurring phenomena when developing various link budgets for satellite communication systems. This being **Galactic Noise**, coming from the galactic center. However, due to the rotation of both the earth and the galactic plane this means that no location on earth sees the center of the galactic plane constantly. Here it is proposed that a new analysis be conducted where depending on the location (latitude and longitude), time, earth's tilt, satellite orbit, and frequency, a dynamic link budget will determine the amount of power to consider for transmission and reception of the corresponding systems. Documentation of the process will be explained throughout the text. Where the problem is thoroughly introduced, and evaluated. Preliminary data is expounded upon helping to show that there is a cyclic nature to this noise source. The area of research conducted is in that of the naval communication, focusing on the the **UHF (Ultra-High Frequency)** band. The design and implementation of the antenna used to collect the data and key points of inspection, with various setups being presented, as well as the curve fitting approach used to predict the appropriate adjustment of problems.

TABLE OF CONTENTS

List of Figures	vii
List of Tables	x
List of Symbols	xi
Acknowledgments	xiv
Chapter 1	
Introduction	1
1.1 The Milky Way	1
1.1.1 Earth's Orbit	3
1.2 Galactic Noise	4
1.2.1 Early Discovery	4
1.2.2 Preliminary Data	5
1.3 Purpose	5
1.3.1 Link Budget	6
1.4 Naval Communications	8
Chapter 2	
Hardware Design and Analysis	9
2.1 Overview	9
2.2 Design Considerations	10
2.3 Parabolic Reflector	11
2.3.1 Parabolic Simulations Measurements	13

2.4	3-Element Yagi-Uda Antenna	14
2.4.1	Yagi-Uda Antenna Simulation Analysis	15
2.5	Radio Telescope	17
2.5.1	Radio Telescope Measurements	18
2.6	Low Noise Amplifier	19
2.6.1	Band-Pass Filter	19
2.7	Data Measurements and Recording Components	20
2.7.1	Power Meter	21
2.7.2	DATAQ	21
2.8	NanoVNA-F	22
2.9	Noise Figure	23
Chapter 3		
	Measurements and Data Collection/Analysis	26
3.1	Measurements Overview	26
3.2	Preliminary Data	26
3.3	Measured Data	27
3.3.1	Daily Comparison	29
3.4	Data Interpretation	30
Chapter 4		
	Software Implementation	32
4.1	Stellarium	32
4.2	Simulation and Measured Data Correlation	34
4.3	Software Defined Radio	35
4.3.1	HackRF One	36
4.3.2	GNU Radio Companion	36
4.4	WinDaq	38
4.5	Matlab	38
Chapter 5		
	Results/Link Budget Analysis	39
5.1	Data Analysis	39
5.2	Curve Fitting	39
5.3	Curve Fitting Results	41
5.4	Link Budget Analysis	43
5.5	Dynamic Link Budget	44

Chapter 6	
Conclusion/Future Work	45
6.1 Future Work	45
6.1.1 Function Completion	46
6.1.2 System Components	46
6.2 Conclusion	47
Appendix A	
Low Noise Amplifiers Data Sheet	48
Appendix B	
Matlab Codes	51
References	55

LIST OF FIGURES

1.1	The celestial sphere with the inclusion of the galactic plane. Here the Earth is not tilting, making its equator equal to that of the celestial plane, however this is not the case throughout the entire year of its orbit around the sun. the galactic plane is more notable being that there is a difference of 63°	2
1.2	The Milky Way with Earth's location inside of the Orion Belt. This photo is taken from article [6].	3
1.3	Dr. Karl Jansky's minimum noise level measured on dipole antennas resonating at 9.31, 17.95, and 21.41 MHz [1]. Each antenna taken measurement during the same 24 hour interval three different times.	6
2.1	The 2.4 meter parabolic reflector used in conjunction with the 3-element Yagi-Uda antenna. Also known as a radio telescope. . . .	12
2.2	Simulation of parabolic reflector excited by 250 MHz center fed dipole antenna. Antenna model (top-left), 3-D gain pattern at 250 MHz (top-right), 3-D gain pattern at 243.7 MHz (bottom left),and the polar plot of the vertical cut of the antenna in the desired direction. It can be seen that the dish vastly improves the directivity of the plot.	14
2.3	Simulation results of the lone 3-element Yagi-Uda antenna simulation. Consisting of the antenna model (top-left), its gain pattern at 250 MHz (top-right), and the polar plot of the of the vertical cut of the antenna at both 250 and 243.7 MHz (bottom).	16
2.4	The S_{11} parameter based off a frequency sweep from 230-350 MHz. This range is chosen to determine whether this Yagi could receive power from the lower frequencies in the UHF band. Although the simulation has proven that it is not capable.	17

2.5	Radio Telescope simulation results. Model (top-right), gain pattern at 250 MHz, gain pattern at 243.7 MHz, and the vertical plot of the polar plot of both frequencies.	18
2.6	Measured Gain Pattern through the use of an Unmanned Aerial Vehicle (UAV), using a software defined radio. Broadcast at a frequency of 244 MHz.	19
2.7	Amplification and the filtering of the signal recieved from the antenna, is shown above. The process is to first amplify the signal through the use of the first LNA, and then to use pass it through a 12 MHz bandpass filter centered at 244.5 MHz. (238.5-250.5 MHz). Once the desired signal in this frequency range has been filtered then, it amplified once again through another amplifier.	20
2.8	Hewlett Packard 437B power meter, used to convert the received analog signal into a digital form. Measured either in watts or dBm.	21
2.9	Data Acquisition Device, used to measure signal from the power meter, along with recording and storing the data.	22
2.10	The NanoVNA-F is used in order to help measure the yagi's parameters. Using a two port network for measurements. Only the first port is put to use, because the reflection coefficient and return loss is deemed necessary for determining whether or not frequency being centered around is optimal.	23
2.11	Diagram of the system layout.	24
3.1	48-hour data recorded by Nick Rooney. It can be seen that there is pattern reoccurring, at a similar time of each day. Thus giving a cyclic nature tenancies.	28
3.2	72-hour data collection of the sky's noise floor. The cyclic nature of galactic noise is prevalent in that the noise floor rises and falls throughout the day.	29
3.3	72-hour data collection broken up into individual days, and plotted in congruent with one another.	30
4.1	Antenna bore sight simulated using Stellarium program. Simulation time 1:24 am on Aug. 6 2021.	33
4.2	Stellarium simulation of the galactic plane entering into the bore sight of the radio-telescope. This part of the simulation being captured at 6:12 pm on Aug. 5, 2021.	34
4.3	Galactic center leaving the bore sight of the radio-telescope. This image is simulated for the date of Aug. 6, 2021 at 5:05 am.	35

4.4	Simulation of the galactic plane exiting the bore sight of the radio-telescope. Simulated for Aug. 6, 2021 at 3:30 pm.	36
4.5	The HackRF One SDR. Very versatile with a half-plex setup. Used to filter and measure the signal collected by the radio-telescope. . .	37
4.6	GNU Radio Companion flow graph used for the processing of the signal being collected from the radio antenna.	38
5.1	Curve fitting (9 degree polynomial) using the 72 hour data. The established curve is adapting to the data set however, it is not ideal for adaptation for future utilization.	42
5.2	Day one five-degree curve fitted model.	42
5.3	Day two five-degree curve fitted model.	43
5.4	Day three five-degree curve fitted model.	43

LIST OF TABLES

2.1	Loss due to active components based on frequencies at 240, 244.5, and 250 MHz.	24
-----	---	----

LIST OF SYMBOLS

R	Resistance	Ω
L	Inductance	H
C	Capacitance	F
H	Magnetic field intensity	A/m
J_c	Conduction current density	A/m ²
D	Electric flux density	C/m ²
ω	Radial frequency	rad/m
f	Temporal frequency	Hz
J_d	Displacement current density	A/m ²
σ	Complex conductivity	S/m
E	Electric field intensity	V/m
ϵ	Complex permittivity	F/m
σ'	Real part complex conductivity	S/m
σ''	Imaginary part complex conductivity	S/m
σ_{dc}	Direct-current conductivity	S/m
ϵ'	Real part complex permittivity	F/m
ϵ''	Imaginary part complex permittivity	F/m
σ_e	Effective conductivity	S/m
ϵ^*	Complex apparent permittivity	F/m
J_{ce}	Effective conduction current density	A/m ²
J_{de}	Effective displacement current density	A/m ²
J_t	Total current density	A/m ²
$\tan(\phi)$	Effective loss tangent	Unitless
ϵ_r^*	Relative complex apparent permittivity	Unitless
ϵ_0	Permittivity of free space	F/m
ϵ'_r	Dielectric constant	Unitless

E_s	Surface electric field intensity	V/m
E_i	Internal electric field intensity	V/m
γ	Complex propagation constant	1/m
μ	Complex permeability	H/m
α	Attenuation constant	Np/m
β	Phase constant	rad/m
μ'	Real part complex permeability	H/m
μ''	Imaginary part complex permeability	H/m
μ_r	Relative complex permeability	Unitless
μ'_r	Real part relative complex permeability	Unitless
μ''_r	Imaginary part relative complex permeability	Unitless
μ_0	Permeability of free space	H/m
J_{ts}	Total surface current density	A/m ²
J_{ti}	Total internal current density	A/m ²
I	Total current per unit width	A/m
Z_s	Surface impedance	Ω m/m
\hat{n}	Unit normal vector	Unitless
β_0	Phase constant in free space	rad/m
τ	Sheet thickness	m
Z_0	Impedance of free space	Ω
S_{21}	Transmission S-parameter	Unitless
S_{11}	Reflection S-parameter	Unitless
R_s	Surface resistance	Ω m/m
X_s	Surface reactance	Ω m/m
δ	Skin depth	m
S	General scattering parameter	Unitless
i	Measurement no.	Unitless
n	Total no. of measurements	Unitless
u	Estimated standard uncertainty of the mean	
U	Expanded uncertainty	
$k_{2,p}$	Two-dimensional coverage factor	Unitless
F^{-1}	Inverse of F CDF	
ν	No. degrees of freedom	Unitless
p	Decimal percentile	Unitless
v	Wave velocity	m/s
N	No. of points	Unitless
Δf	Frequency step	Hz
Δt	Time step	s
F_{start}	Start frequency	Hz
F_{stop}	Stop frequency	Hz

d_1	Spacer 1 thickness	m
ϵ'_{r1}	Dielectric constant of spacer 1	Unitless
Z_1	Spacer 1 impedance	Ω
Z_L	Load impedance	Ω
Γ	Reflection coefficient	Unitless
Z_{Lt}	Transformed load impedance	Ω
β_1	Phase constant in spacer 1	rad/m
Z_{eq}	Equivalent impedance	Ω
Y	General admittance quantity	S
Z	General impedance quantity	Ω
Y_s	Surface admittance	Sm/m
G_s	Surface conductance	Sm/m
B_s	Surface susceptance	Sm/m
Y_{Lt}	Admittance of transformed load impedance	Sm/m
B_{eq1}	Equivalent susceptance of single-layer CAA	S
Z_{s1}	Surface impedance of sheet 1	$\Omega\text{m/m}$
Z_{s2}	Surface impedance of sheet 2	$\Omega\text{m/m}$
Z_2	Spacer 2 impedance	Ω
d_2	Spacer 2 thickness	m
Z_{eq1}	Equivalent impedance of layer 1	Ω
Z_{eq1t}	Transformed equivalent impedance of layer 1	Ω
Z_{eq2}	Equivalent impedance of two-layer CAA	Ω
G_{s2}	Surface conductance of sheet 2	Sm/m
B_{s2}	Surface susceptance of sheet 2	Sm/m
B_{eq2}	Equivalent susceptance of two-layer CAA	S
ϕ	Measurement angle	$^\circ$
Z_c	Impedance of capacitor	Ω
d	Arbitrary spacer thickness	m
λ	Wavelength	m
Z_w	Wave impedance	Ω
z	Arbitrary real output variable	
x	Arbitrary real input variable	
\mathbf{z}	Arbitrary complex output variable	
\mathbf{x}	Arbitrary complex input variable	

ACKNOWLEDGMENTS

I would like to thank the Applied Research Laboratory ARL, for designating me as a Walker Fellow, and providing funding for my research. Along with giving me opportunity to work along world class researchers, such as Erik Lenzing and Elliot Riley, who brought to my attention this problem. In doing so I have grown so much both academically, and professionally. The guidance of these two provided me with the structure needed to complete various task embedding in me the confidence to do so.

Next are my advisors Dr. Julio and Dr. James Breakall. Both of these gentlemen have been very patient and giving me the constructive criticism needed to grow, and understand the things that I didn't. This and challenging me to leave my comfort zone, and seeking to be more adept at solving problems.

I would also like to thank the Dr. Stephanie Preston for her guidance in navigating graduate student life. With her guidance I have been able to overcome imposter syndrome.

I also would like to thank Will Fletcher and Alex Yuan for being out in the field conducting tests along with me. All while filling in any gaps of knowledge that came along with being a novice.

Lastly but definitely not least Dr. Harry Lenzing, for the giant head start you gave me in helping be to understand how galactic noise and link budgets work.

Thank you all.

This thesis is supported by the Applied Research Laboratory (ARL) at The Pennsylvania State University (PSU). With an award totaling the amount of tuition and fee requirements of the university for a two year period. The contents of this document does not necessarily represent the official views of, nor an endorsement, by ARL nor PSU. For more information please visit esm.psu.edu.

DEDICATION

I would like to dedicate this thesis to my family and friends for all of your support. To my niece, nephews and younger cousins, I challenge you to chase your dreams and be curious. To my parents thank you so much for helping throughout all of the years that I have spent mainly as a student. All while letting me know that I can do all things through Christ who strengthens me.

CHAPTER 1

INTRODUCTION

1.1 The Milky Way

Most know that there are various universes, and each contain galaxies. There are various galaxies that have been discovered, with the Milky Way, the most familiar being that is the one we inhabit. Galaxies are defined as a massive collection of stars, stellar remnants, interstellar gases, dust and dark matter. Dr. Edwin Hubble's 1926 paper, study [4], classifies galaxies by their shape. These are elliptical, lenticular, spiral, and irregular. With the Milky being a spiral galaxy, this type will be elaborated upon. Spiral galaxies tend to be likened unto a flattened disk with arms. Normally there being two arms that are tightly or loosely bound to its galactic center, consisting of a concentration of stars [5]. The Milky Way similar to the other galaxies in the universe was formed as a remnant of the Big Bang. With its center being the black hole Sagittarius A. The common approach when modelling the galaxy is to use a celestial sphere that encompasses the entire galaxy, or just a section of it, to help with referencing different celestial bodies. Figure 1.1 from article [3], shows the galactic plane in reference to the celestial sphere. This model is in reference to the Earth's equatorial plane, symbolizing an orb that contains the Milky Way with respect to the Earth's orientation. It can be inferred that the two planes do not align, thus proving that the various locations on the globe do not each view the galactic plane. However, this figure is not enough to interpret the

Earth's location in the Milky Way. From this image one would conclude that the

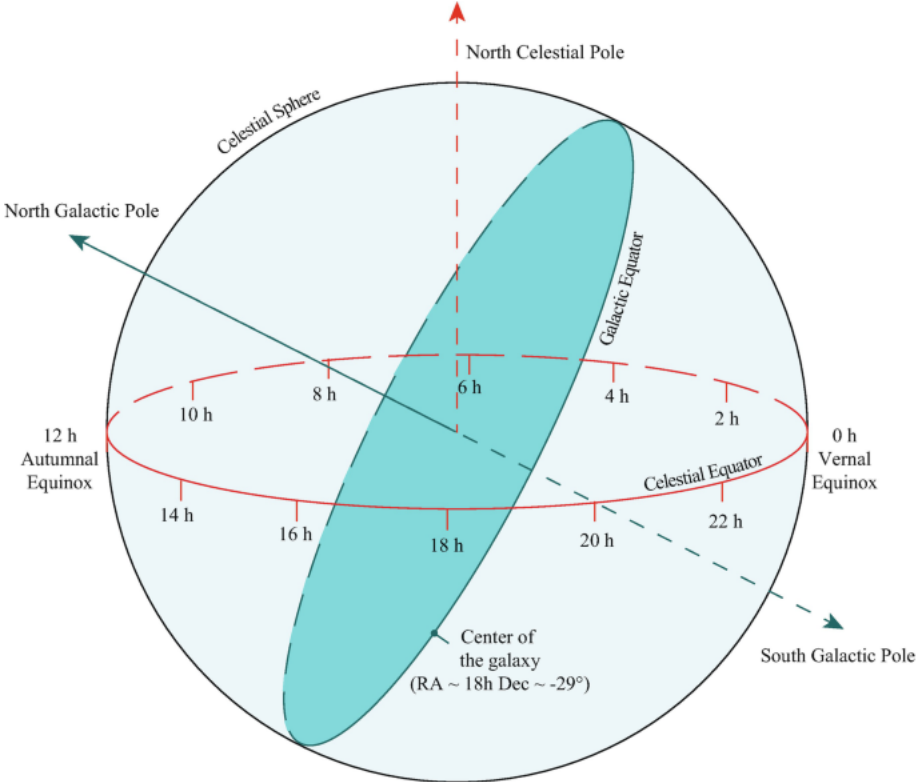


Figure 1.1: The celestial sphere with the inclusion of the galactic plane. Here the Earth is not tilting, making its equator equal to that of the celestial plane, however this is not the case throughout the entire year of its orbit around the sun. the galactic plane is more notable being that there is a difference of 63°.

Earth is at the center of the galaxy however, as stated before Sagittarius A is the center point. The model provided in Figure 1.2 allows for this to be seen. It has been determined through prior studies that the Earth lies in one of the spiral arms of the Milky Way. This arm being known as the Orion Arm, with the solar system being approximately two thirds out from the center of the galaxy. In order to get a feasible idea of the location, the celestial sphere is taken into account for latitude purposes. This is because the spiral galaxies are often referenced as flat, however that is not the case, but in consideration to its other dimensions it is relatively small.

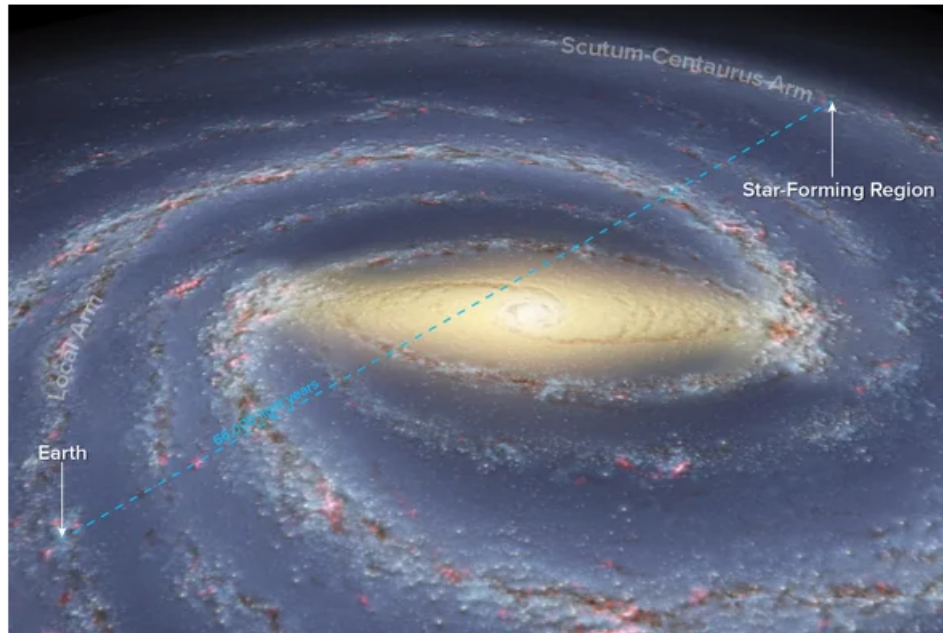


Figure 1.2: The Milky Way with Earth's location inside of the Orion Belt. This photo is taken from article [6].

1.1.1 Earth's Orbit

Another parameter that needs to be taken into account, is the Earth's orbit. It is common knowledge that the solar system is heliocentric. With all of the planets orbiting the sun. However, the Earth's is different in that it has an elliptical orbit, it tilts, and also constantly rotates. Each of these actions having there own significance in the daily occurrences of the planet. For instance an elliptical orbit means that as the Earth travels around the sun in a circular fashion. However, at some points throughout the year the Earth orbits closer to the sun, relatively to the distance between the two during farther orbiting periods. The spinning is consistent, neither slowing down nor speeding up. Tilting occurs along the equator, thus creating the environments along with the varying seasons throughout the globe. With locations close to the equator having roughly the same conditions throughout the year. Unlike those that are further away. All three orbiting parameters are looked at further throughout the text for research purposes. All of these parameters have a cyclic nature, making their future occurrences predictable. Allowing for technological advancement in the fields of astronomy, space exploration, renewable energy, and communication. With communication playing a key aspect in each of

the fields. When looking at figure 1.1 it shows that the Earth's equatorial plane and that of the galactic plane have a difference of 63° . Even though the Earth is at a constant tilt of 23.4° . Taken into consideration the conjunction of all these natural occurrences allows for better predictions to be made when, developing a link budget system in compensation of galactic noise.

1.2 Galactic Noise

Communication has constantly changed over the millennia. Different tools and methods have constantly improved the way one may connect with another. However, none has had the sheer impact of the satellite. Satellites have had a major impact on everyday life, allowing for global connection in milliseconds. Being very versatile there are many uses for this technological advancement, such as broadcasting, climate observation, in numerous forms of remote sensing, and defense. Being able to communicate effectively as well as efficiently over vast distances is of great importance. It is for this reason and for safety purposes that the radio frequency spectrum has been split into different bands and allocated for specific reasons. However, no matter what frequency may be of use there still exist noise. This phenomena has come to be known as any fluctuation in a signal that may hinder or obscure it. Noise comes from many different sources in electromagnetics, whether it be man made or of natural occurrences. For the purpose of this study a natural occurrence stimulating from **Sagittarius A**, the black hole at the center of the Milky Way galaxy is of great importance. This being the **Galactic Noise**.

1.2.1 Early Discovery

During the early 1900s radio communication had taken a significant leap forward, and many interests were formed. In the summer of 1931, Dr. Karl Jansky [1], a radio frequency engineer for Bell Telephone Laboratories, set out to find noise sources that could interfere with radio signals. Many of these noise sources at the time were man made consisting of, the popular rail-ray systems, electric motors from the vehicles, and power lines that delivered power to many businesses and homes. Once the normal hours of a traditional work day was completed, noise by man made sources vastly decreased. However, one source seem to be prevalent,

dependent on the direction an antenna is observing at a certain time of day. It was first believed that the sun was the major contributor of this interference. Further studies in 1932 showed that these disturbances were notably higher when pointed at the galactic plane, and even higher when looking towards its center. It is here that Dr. Jansky denoted the origin of this noise is at a fixed location, Sagittarius A. In order to understand noise from interstellar origins, it is good to look at the make up of the universe. Thus seeing the nature of how many celestial phenomena may affect even the most minute of objects, systems, or other natural occurrences.

1.2.2 Preliminary Data

The experiments in [1] were conducted using three dipole antennas. Wavelengths of 14 (21.41 MHz), 16.7 (17.95 MHz), and 32.2 (9.31 MHz) meters. In order to obtain accurate measurements of the noise level, tests were conducted throughout the entire day with night time data being more desirable in order to better characterize galactic noise. Graphical representation of the noise levels are shown in the figures below for each of the dipole antennas. Figure 1.3 shows the measurements taken at 21.41 MHz. Each curve represents a different twenty-four hour period the measurement was taken. With the first being taken from midnight on January 27 to midnight of the 28. The second being between February 3-4, next, February 10-11, and lastly February 17-18, all in the year 1937. One can see that not all of the curves are continuous, although notable it is not elaborated upon in the presented paper. Looking closely there is a cyclic nature to the noise levels. At certain points throughout the day this noise is more prevalent, and above the desired noise floor of -48 dBm.

1.3 Purpose

Galactic noise has become a well known nuisance in the satellite communication community. Mainly affecting receivers throughout the globe, facing orbital vehicles. This is because these antennas are facing the sky in order to receive signals from satellites. However, they noise from the **Cosmic Microwave Background (CMB)** is being collected degrading the **Signal-to-Noise Ratio (SNR)**. For the signal to be received it must be above a noise floor, each system typically having

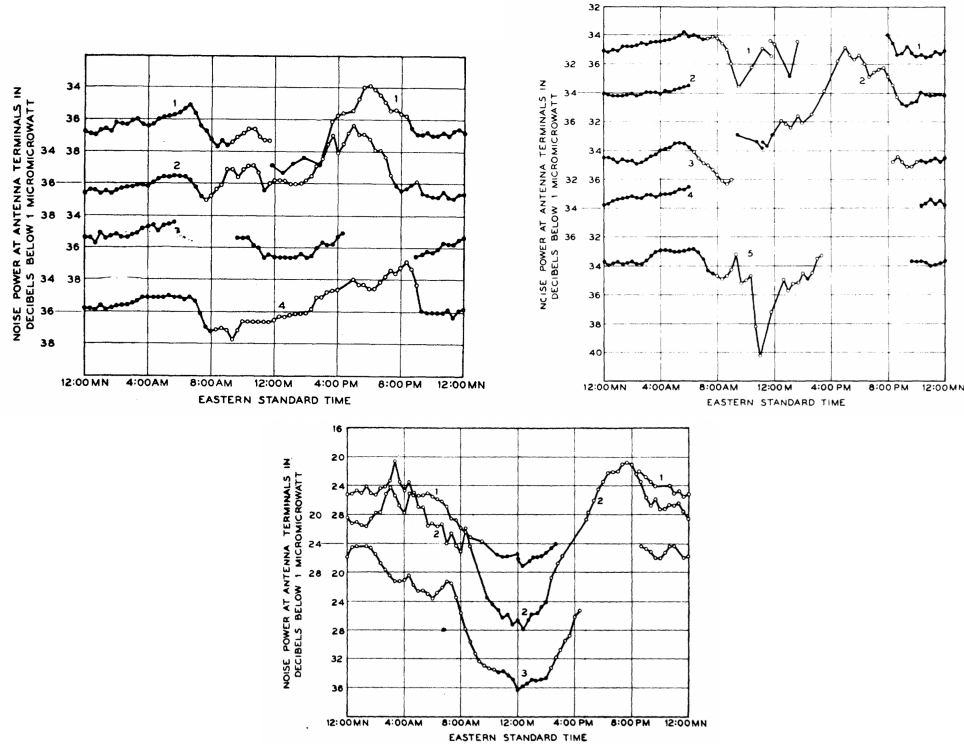


Figure 1.3: Dr. Karl Jansky’s minimum noise level measured on dipole antennas resonating at 9.31, 17.95, and 21.41 MHz [1]. Each antenna taken measurement during the same 24 hour interval three different times.

there own noise floor depending on the amount of amplification being done. It is for this reason a link budget is developed ensuring that once all the losses have occurred what the signal’s strength is when reaching the receiver.

1.3.1 Link Budget

Link budgets change depending on medium, distance, and any other losses that may occur between transmission and reception. The following equation shows how a link budget is calculated.

$$P_{RX} = P_{TX} + G - L \tag{1.1}$$

Where the variables dB represent:

- P_{RX} is the Power received.

- $P_T X$ is the power transmitted.
- G is the total gain.
 - Referring to any amplification process the signal may go through before reaching the receiver.
- L is the total loss of signal power before reception.

Common losses are the following:

- Free Space Path Loss (FSPL)
Calculated using the following equation:

$$FSPL = \left(\frac{4\pi d}{\lambda}\right)^2 \quad (1.2)$$

- Hydrometeors
 - (i) Rain
 - (ii) Snow
 - (iii) Sleet
 - (iv) Hail
- Atmospheric Loss
- Ambient Noise
- Man-Made
- Natural Occurrences
 - (i) Solar
 - (ii) Rainfall Rate
 - (iii) Microwave Cosmic Background
 - (iv) Galactic Noise

All of these play a factor when incorporating losses. However the focus is on galactic noise because there are various studies showing its existence however, systems do not always accurately account for this form of loss. Which can have consequences for different periods throughout the day.

1.4 Naval Communications

This studies looks to improve the link budget analysis for naval communication. Although they utilize impressive systems, there is always room for improvement, especially efficiency wise. Most of these systems either overcompensates for galactic noise, or it doesn't compensate for it at all. Overcompensation occurs because studies show that throughout the day the noise floor rises to a certain point. So those in charge of the communication link designs, takes into account only this maximum factor for galactic loss. Which is wasteful for other points throughout the day, with that power not being of any use. In the case of no compensation being accounted for this means that, communication failures will occur when the signal to noise ratio is close to the noise floor, falling below it caused by an increase of the noise floor due to galactic noise. It is for this reason that this study proposes in place of a static link budget, a dynamic one be used that takes into account the cyclic change of the noise floor based on the cyclic nature of galactic noise. This is done using a **Radio Telescope** to accurately depict this daily occurrence and, then produce a model that gives a changing value for the galactic noise loss based on the time and location of the given link.

CHAPTER 2

HARDWARE DESIGN AND ANALYSIS

2.1 Overview

For accurate measurements to be taken, hardware considerations must be taken into account. Compared to when Dr. Jansky first discovered the galactic noise interference, there are a lot more things to take into noise sources to taken into account. For instance the increase in the use of wireless communication, being in the age of the **Internet of Things (IoT)**. Many different devices communicate with one another, thus furthering the need to determine the link budget for many different devices. However, for satellite communication this problem is not so much of a problem mainly because most land receivers are pointed at an angle that allows for most of these sources to not affect the signals being transmitted to them. This is shown to be true later in the studies, where the antenna that is used points directly at the sky. Naval vessels tend to use **Omni-directional SATCOM** satellites. Although very versatile, they still face times when communication links are not always at optimum levels, and even points when they are not able to communicate effectively. Even though the actual antenna/receiver systems used are not used, the equipment used does suffice, and efficiently detect the noise source being sought after. Also needed to be noted is, with there only being a need to collect data on galactic noise, transmitting is not need, making this a half-duplex system, that collects data passively.

2.2 Design Considerations

Being that the Applied Research Lab provided the system materials need for this project, it must be noted that the system used was inherited from a previous project similar to this one. However, changes to the system was discussed, and suggested. This section serves to highlight some of those changes. There are many different types of antennas that have become popular in modern times for numerous reasons. Although, a plethora to choose from, not all would be optimal. Being that the frequencies of interest lie within the UHF band, the aperture's size serves a significant role. For instance high directivity is needed in order to direct enough of the signal precisely onto the element collecting and transferring the power to the measuring devices. Directivity is the maximum gain in a given direction by an antenna in its far field. Equation 2.1 shows how to calculate directivity.

$$D = \frac{P(\theta, \phi)_{max}}{P(\theta, \phi)_{av}} \text{ (linear)} \quad (2.1)$$

$$D(dB) = 10\log_{10}D \quad (2.2)$$

With theta and phi expressing the degree of azimuth and zenith respectfully. Another factor is the antenna's bandwidth being that the UHF-Band covers a range from 300 MHz to 3 GHz. An early thought was to use a microstrip patch antenna due to its ease of production, robustness, along with being able to be designed with a high bandwidth. However, it didn't seem to be optimal being that it the directivity needed would not be fully achievable. The most efficient way to get a high directivity would be to use an aperture that could both collect and direct radiated energy. So the first consideration when looking at other design ideas, was to use a horn antenna in conjunction with a wave guide with a cut-off frequency of 200-300 MHz. The thought process is that this would allow for frequencies at ande higher than this range to be collected only, thus having a pretty good band with. However, this proved to not be a good suggestion being that it would involve a large apparatus that is not readily purchase-able. With the waveguide being one of the hardest to find. Thus the original system design was used and worked very well. A list of the equipment is below, followed by the sections explaining the roles each individual part played in the procuring of the desired results.

- Parabolic Reflector
- Yagi-Uda Antenna
- NanoVNA-F
- Low Noise Amplifier
- Bandpass Filter
- Power Meter
- DATAQ USB
- Software-Defined Radio
- Coaxial Cable

2.3 Parabolic Reflector

Parabolic reflectors are well known and used extensively for the gathering of electromagnetic waves. What makes this part of the antenna so essential is that it collects and directs the gathered waves that hit it. These waves no matter where they hit on the surface of the aperture, manages to reflect to a focal point determined by the design of the aperture. A 2.4 m aperture is selected, allowing for wavelengths of up to 2.4 meters to be captured. With a medium being air, the waves coming into contact with the dish, has a velocity equivalent to that of the speed of light. Using this the minimum frequency can be determined, it should be inferred that higher frequencies having a smaller λ are collected as well. The smaller the λ is compared to the aperture area the higher the amount of gain, and the narrowing of the beam-width. The following equations were used in confirming that the aperture size is sufficient.

$$c_0 = \frac{1}{\sqrt{\mu_0 \epsilon_0}} \approx 2.99 \times 10^8 \frac{m}{s} \quad (2.3)$$

$$c_0 = \lambda f \Rightarrow f = \frac{c_0}{\lambda} \Rightarrow f = \frac{2.99 \times 10^8}{2.4} \approx 124.6 \text{ MHz} \quad (2.4)$$

This would suffice when looking to gather galactic noise affecting UHF band frequencies. In doing so smaller beamwidths are achieved in the process, granting the desired directivity. With high gain being at the focal point for collecting



Figure 2.1: The 2.4 meter parabolic reflector used in conjunction with the 3-element Yagi-Uda antenna. Also known as a radio telescope.

purposes, observations were conducted at both 250 MHz and 243.7 MHz. Although both being in the VHF band, the frequencies of interest for military communication ranges from the higher VHF to the UHF band. The theoretical gain for an antenna of these dimensions, as well as operating under the specified parameters, is calculated using the following equations:

$$focal\ point = \frac{r^2}{4a} = \frac{1.2^2}{4(37.5)} = 97.3\ cm. \quad (2.5)$$

$$\lambda = \frac{c_0}{f} = \frac{2.99 \times 10^8}{250 \times 10^6} = 1.196\ m \quad (2.6)$$

$$\lambda = \frac{c_0}{f} = \frac{2.99 \times 10^8}{243.7 \times 10^6} = 1.227 \text{ m} \quad (2.7)$$

$$G = 10 \log_{10} k \left(\frac{D\pi}{\lambda} \right)^2 \quad (2.8)$$

$$G_{250} = 10 \log_{10} .5 \left(\frac{2.4\pi}{1.196} \right)^2 = 12.98 \text{ dBi} \quad (2.9)$$

$$G_{243.7} = 10 \log_{10} .5 \left(\frac{2.4\pi}{1.227} \right)^2 = 12.76 \text{ dBi} \quad (2.10)$$

2.3.1 Parabolic Simulations Measurements

In order to gain an understanding of the system, simulations of the radio telescope were conducted, with the first being that of the dish. Where the goal is to determine the gain pattern of the dish to ensure the feed-point is in the optimal location. Using the same dimensions CADFEKO is used to simulate the dish, to get an idea of the amount of gain, along with a visual of the beam formation. Figure 2.2 shows the parabolic dish being excited by a single center fed dipole antenna, operating at at 250 MHz. In order to determine desired effects of the dish, it must be excited by another driven element. In this case it is the same driven element used in the to drive the Yagi-Uda antenna analyzed in section 2.2.2. When looking at the simulation results in Figure 2.2 is can be seen that dipole is placed at the focal point of the dish, in the center approximately 97.3 cm away from its surface. Next a simulation with a frequency sweep from 230-250 MHz is conducted, where the gain for each frequency is can be seen, just as in theory a correlation between the gain frequency occurred where as the frequency increased, so did the gain in the desired direction at 0°. It is here that the maximum gain is found being 12.2 dBi and 12 dBi at 250 and 243.7 MHz respectively. When using just a center fed dipole antenna more of a donut shape occurs, how and where the peak is that would be a null. Although quite efficient for the task at hand, a major concern for the dish is its edge. Round edges tend to allow for more diffraction when incident upon. Unlike a sharper edge, the waves tend to bend easier around the edge. This effect is explained in the **Uniform Theory of Diffraction (UTD)**, which is used to explain how electromagnetic waves propagate through various terrains. For this study this effect is not one that affects the collected data significantly, so not much insight is taken. However, during simulation is was seen that very little of the energy actually bent around and got underneath the structure, as can be

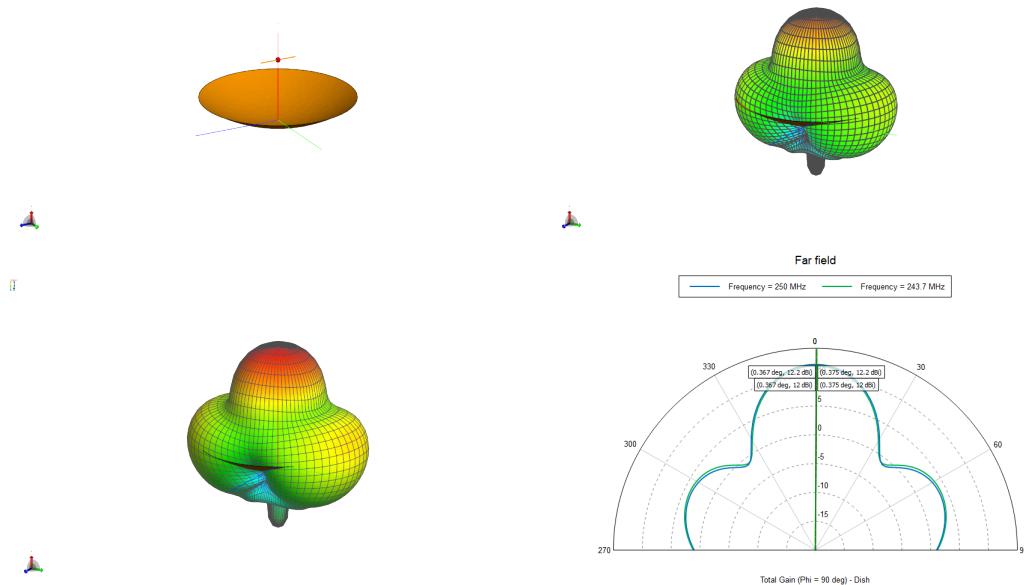


Figure 2.2: Simulation of parabolic reflector excited by 250 MHz center fed dipole antenna. Antenna model (top-left), 3-D gain pattern at 250 MHz (top-right), 3-D gain pattern at 243.7 MHz (bottom left), and the polar plot of the vertical cut of the antenna in the desired direction. It can be seen that the dish vastly improves the directivity of the plot.

inferred from the 3-D gain patterns via color implementing the intensity of the energy in propagating in a given direction. Overall the gain does show significant improvement.

2.4 3-Element Yagi-Uda Antenna

In order to receive and collect the signals for measurement, an antenna is needed, one that could do so efficiently, as well as at a lower production point. The Yagi-Uda antenna is chosen for the task, and performed quite well. What makes this type of antenna so unique is that it is basically a linear dipole antenna array, with only a single driven element, in this case a 250 MHz center fed dipole is used as stated in the previous section. The length of this driver being 54.3 cm. Yagi's are unique in that they are great for narrow beam-forming. Using the basic dipole antenna theory, where a half wave dipole antenna is used in to capture the waves

incident upon it. With the desired frequency being selected and the associated λ is determined. The length of the dipole is half that of the wavelength, but split in the middle where it is excited by a source. This is where the induced current from the EM waves incident upon it is collected and directed to the measuring devices. To make sure as much of the energy as possible is directed to the receiving element efficiently, another element called a deflector is placed behind it. Deflectors are normally slightly longer than the main element, contributing to the focusing of the antenna radiation pattern. The deflector is of length 55.3 cm. Along with the deflector a director is placed in front of the driven element, thus furthering the focus of the beam. These help in making sure most of the collected power is being recorded. Adding more deflectors and directors to the design would allow for further narrowing of the beam, however there would be drawbacks efficiency-wise. Drawbacks of the Yagi is similar to that of most linear antennas, that being its bandwidth. When first assigned this research, the previous user of the antenna believed it to operate optimally at 250 MHz, this was not the case. The return loss was actually higher than the commonly accepted -10 dB. This may have been due to the many environmental factors. It was discovered that at 243.7 MHz the return loss was approximately 1% at -19.21dB. Thus when conducting measurements the latter frequency is chosen. Figure 2.1 shows the entire antenna apparatus, that includes both the Yagi and parabolic reflector dish.

2.4.1 Yagi-Uda Antenna Simulation Analysis

Using CADFEKO and POSTFEKO an analysis of the system was done. Figure 2.3 shows the results of these simulations. Where the model consist of the antenna point towards the where the parabolic is intended to be. It can be seen via the second figure displaying the gain pattern a resemblance to the traditional center fed dipole. However, most of the energy is being directed away from the driver and reflector. Only the plot of from the 250 MHz simulation is shown being the plot from 243.7 MHz. The polar plot shows that the maximum gain is toward 180° , being 6.77 dBi and 6.57 dBi at 250 MHz and 243.7 MHz respectively. Another simulation ran on this yagi is the s-parameter where the reflection coefficient is measured via the S11 parameter. Here it can be seen from the frequency sweep this antenna can be used effectively from 230 MHz to 266 MHz, thus having an

effective bandwidth of 36 MHz equalling 14.5% with the center frequency being 248 MHz. The simulation having been conducted multiple times suggest that this particular antenna is resonant at 257.9 MHz, having a reflection coefficient of -35.86 dB. However, as stated before when taking the actual physical measurements this was not the case. The S_{11} parameter is shown in Figure 2.4. The simulation analysis shows that the Yagi is in fact operating efficiently within the parameters it was designed for. However, with a goal of characterizing a dynamic link budget for communication systems operating within UHF frequencies, this antenna will not suffice. It can be seen that frequencies above 266 MHz the accepted return loss of -10 dB will not be achieved. With almost no power being sustained at 294.7 MHz where the s11 parameter is -0.31 dB. It is proposed that a log periodic antenna is used to incorporate the entire UHF band.

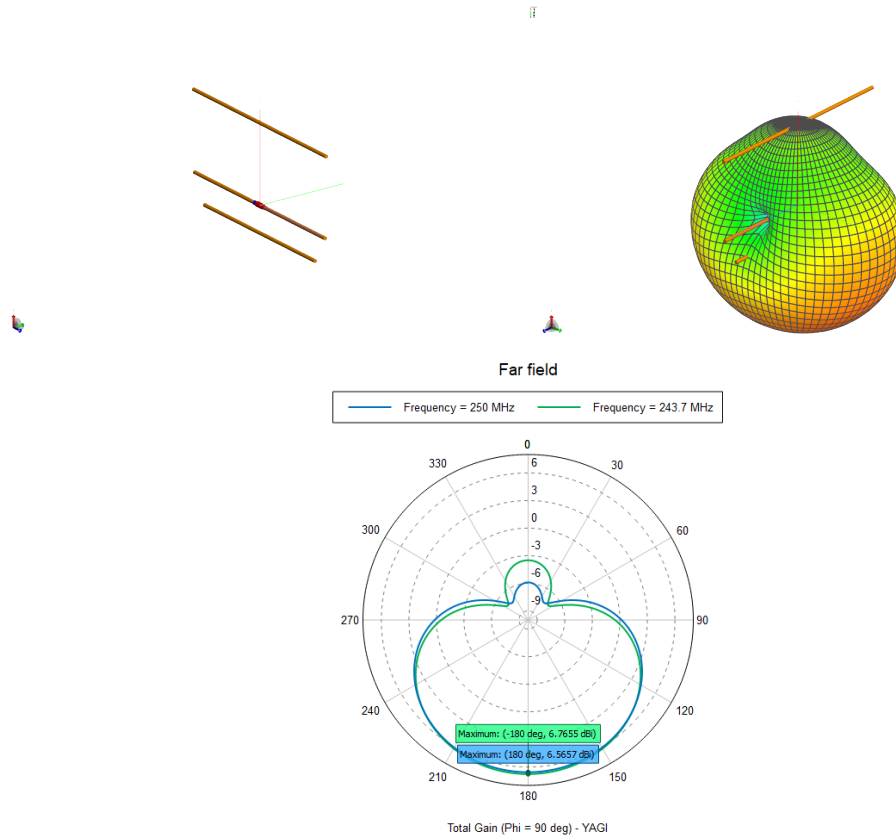


Figure 2.3: Simulation results of the lone 3-element Yagi-Uda antenna simulation. Consisting of the antenna model (top-left), its gain pattern at 250 MHz (top-right), and the polar plot of the of the vertical cut of the antenna at both 250 and 243.7 MHz (bottom).

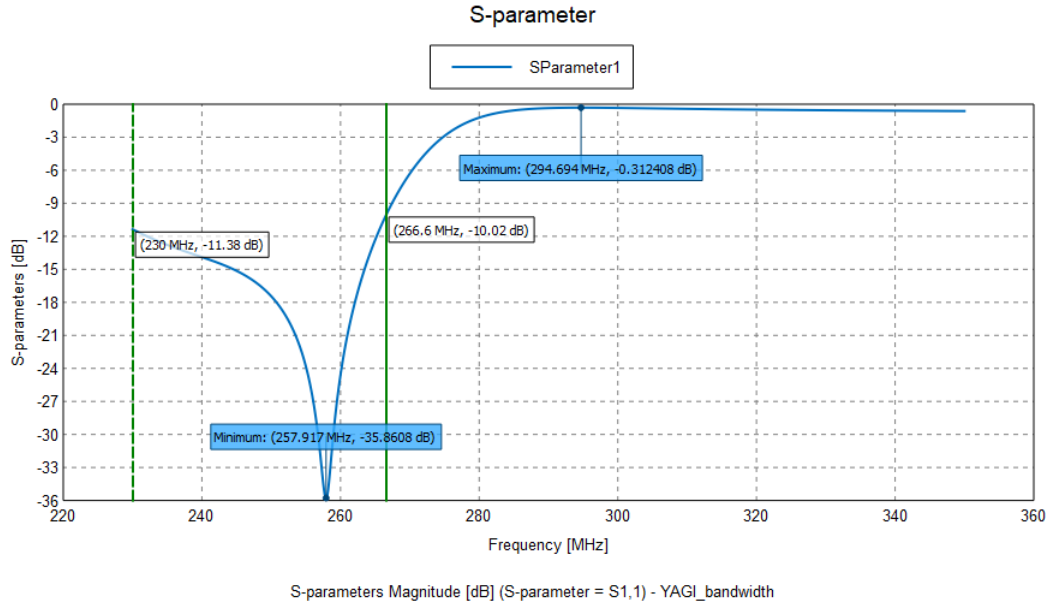


Figure 2.4: The S_{11} parameter based off a frequency sweep from 230-350 MHz. This range is chosen to determine whether this Yagi could receive power from the lower frequencies in the UHF band. Although the simulation has proven that it is not capable.

2.5 Radio Telescope

Observing using a passive approach, means a **Radio Telescope** is needed. A radio telescope is used to observe radio signals coming from space. In order to effectively do this the models are used in conjunction with one another. Making the Yagi-Uda the excitation element for the dish. Figure 2.5 shows the simulation results for the design. It can be seen at both simulation frequencies the goal of sending as much power as possible into the driver is achieved. The major lobe has a gain of 13.37 dBi and 13.59 dBi at 250 and 243 MHz respectively. In doing so the minor lobes have decreased from approximately 8dBi to 4 dBi, along with creating nulls in at both frequencies. This is achieved by using focusing any received power by the Yagi elements into the dish, honoring the law of reflection, where the angle of reflection is equal to the angle of incidence. This contributing to why all reflected power is focused at focal point, helped to further increase the gain.

2.5.1 Radio Telescope Measurements

Confirmation that the radio telescope's gain pattern is similar to those from the simulations. Figure 2.6 shows actual gain pattern that was taken using an unmanned aerial vehicle (UAV). The drone flew over the radio telescope while a HackRf One attached to a dipole antenna is being used to measure the energy being propagated from the setup. It should be noted that in order to do this a signal generator is attached to the antenna through the use of a coaxial cable. Supplying a 3 dB signal at 244 MHz, the antenna emits forming the gain pattern shown in Figure 2.6. The pattern is quite close to that produced in **POSTFEKO**. Although not quite exact, this is to be expected when doing practical measurements. Also the gain at the different peaks cannot be measured using this method, but the same overall pattern does exist. Noticeable differences are the nulls not being as distinct, along with the pattern edges not being smooth.

figure

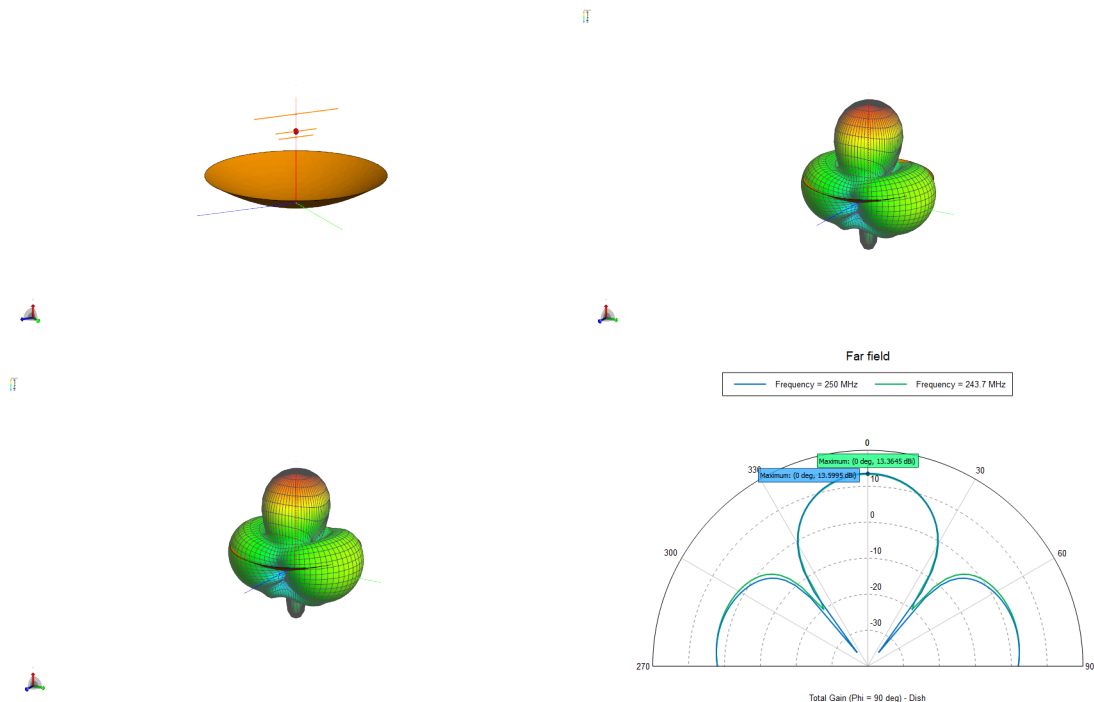


Figure 2.5: Radio Telescope simulation results. Model (top-right), gain pattern at 250 MHz, gain pattern at 243.7 MHz, and the vertical plot of the polar plot of both frequencies.

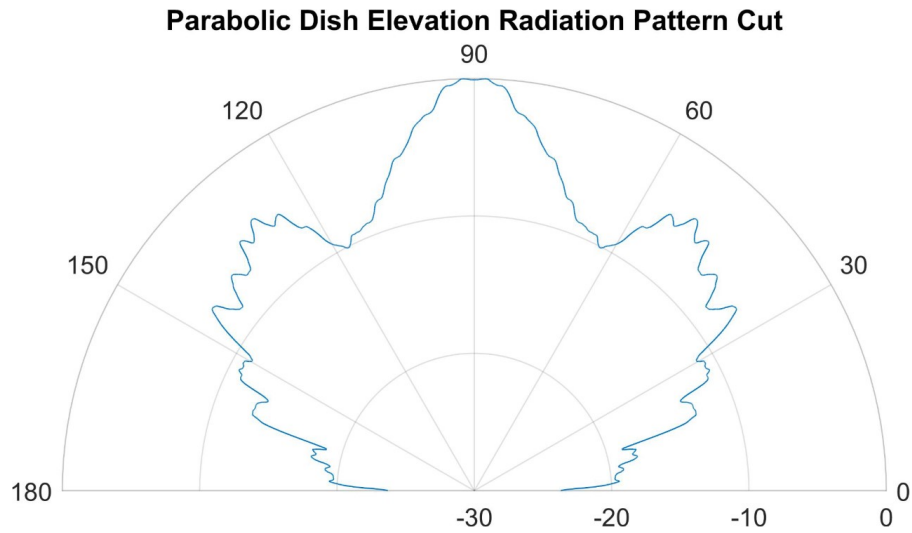


Figure 2.6: Measured Gain Pattern through the use of an Unmanned Aerial Vehicle (UAV), using a software defined radio. Broadcast at a frequency of 244 MHz.

2.6 Low Noise Amplifier

Being that the signal being captured is of small magnitude, in order for accurate measurements to be taken, the signal must be amplified. This is achieved via a **Low Noise Amplifier (LNA)**. LNAs are crucial to the design in that it is an active circuit element that does not add much thermal noise to a circuit. Thermal noise is due to the agitation of electrons, basically all circuits produce unwanted noise. Unlike passive elements such as resistors, capacitors, and inductors, these devices do not add in thermal noise to a circuit because they do not add any additional power. Here in the design of the receiver there are two LNAs, each supplying 30 dB of gain to the signal. The layout of the of the entire system is shown in Figure 2.7.

2.6.1 Band-Pass Filter

A critical piece in the sifting of the signals being collected is the **Band-Pass Filter**. This component function is to filter the frequencies being collected by the aperture. Having a center frequency of 244.5 MHz with 12 MHz of range (238.5-250.5 MHz), Thus being able to supply the desired frequencies. Similar to the LNAs this device adds to the noise figure of the overall system. However, the amount of noise is

dependent upon frequencies, shown in table 2.1.

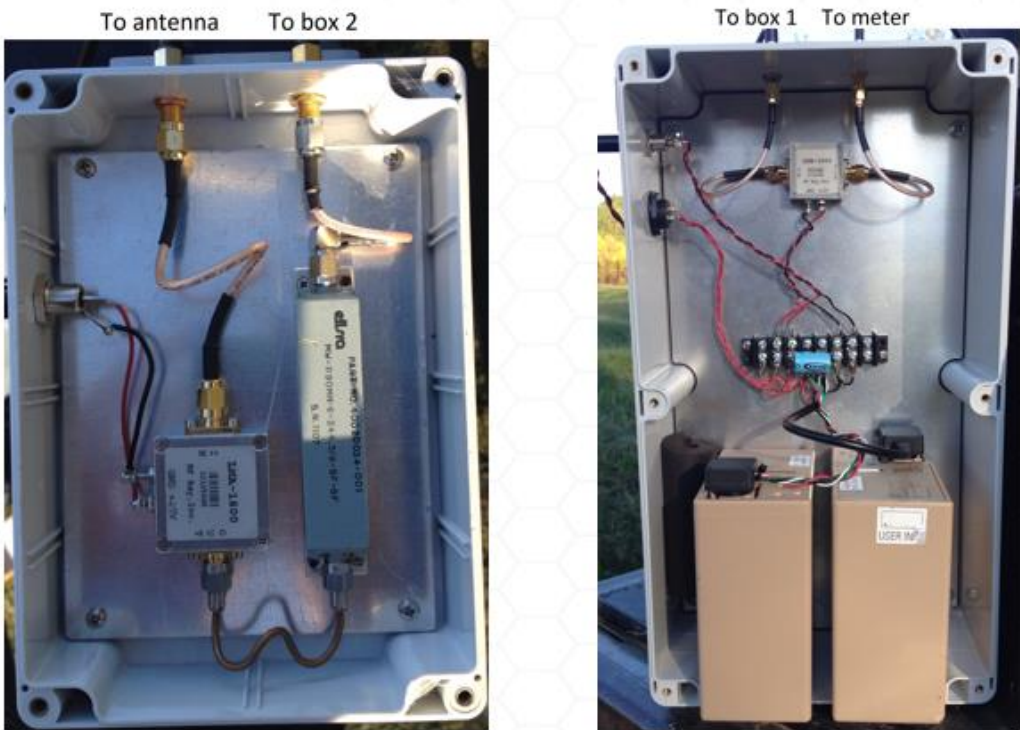


Figure 2.7: Amplification and the filtering of the signal received from the antenna, is shown above. The process is to first amplify the signal through the use of the first LNA, and then to use pass it through a 12 MHz bandpass filter centered at 244.5 MHz. (238.5-250.5 MHz). Once the desired signal in this frequency range has been filtered then, it amplified once again through another amplifier.

2.7 Data Measurements and Recording Components

The previous devices play a key role in collecting and transferring the sought after frequencies. In order further work with the data it must be converted from an analog signal to a digital one. Once this is achieved it can be stored, and used for the study. The following two components are used for these tasks. First beginning with the conversion from analog to digital, through the use of a power meter.

2.7.1 Power Meter

Once the signal has been amplified and filtered it is measured using the **Hewlett Packard 437B** power meter. This connection is made using a coax-Type-N converter. Where the signal is converted into power, and is measured either in watts or decibels. Before measurements are taken calibration is done in order to determine power of the observed frequency.

2.7.2 DATAQ

Upon measuring the data from the power meter, it needs to be recorded and stored for observation purposes. The **Data Acquisition Device (DATAQ)** is used for these purposes. In doing so the power received from the power meter is measured, and recorded for later use. Once it has been stored the data is exported to an excel file containing the power, date/time of the received signal. Various recordings of measurements have been stored. These records of the measured data will be shown in the latter chapters. Figures 2.8 and 2.9 show the power meter and DATAQ respectively.



Figure 2.8: Hewlett Packard 437B power meter, used to convert the received analog signal into a digital form. Measured either in watts or dBm.



Figure 2.9: Data Acquisition Device, used to measure signal from the power meter, along with recording and storing the data.

2.8 NanoVNA-F

In determining the performance of the antenna, a **Vector Network Analyzer (VNA)** is used. One of the main concerns is the return loss, in order to measure how effectively the antenna is at gathering energy for specific frequencies or in a frequency range. This is done by a signal with a certain amount of power being sent into the antenna via the S11 port (Scattering Port 1). The ones signify that power is being sent through port one and being measured at port one as well. The returning power ideally would be equal to that going in, but there are various forms of losses occurring. However, the frequency at which the least amount of power is lost, is known as the resonant frequency. Thus letting the user know which frequency their antenna would be the most efficient at. The NanoVNA-f was chosen for this task mainly do its size, dependability, and portability. There were some problems in that its touchscreen capabilities were not always calibrated properly. Thus making it hard to calibrate when conducting tests. Calibration was needed in order to get accurate parameter measurements for the return loss. The **S-O-L-T** short, open, load (50Ω), and through method was used. Figure 2.2 shows the NanoVNA-F, and the schematics of the ports.



NanoVNA-F™

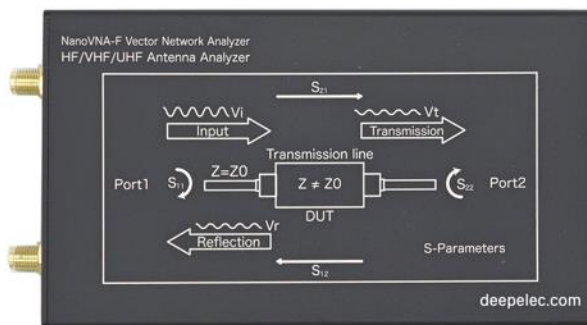


Figure 2.10: The NanoVNA-F is used in order to help measure the yagi's parameters. Using a two port network for measurements. Only the first port is put to use, because the reflection coefficient and return loss is deemed necessary for determining whether or not frequency being centered around is optimal.

2.9 Noise Figure

In order to determine that the signal being measured is accurate, noise from various elements throughout the system must be taken into account. This noise needs to be accounted for, so that it can further degrade the signal to noise ratio. The noise produced by the components in a system is known as its **Noise Figure (NF)**. The NanoVNA-F is used to measure these losses. This process was done using a 20 dB attenuator in case too much power is being inserted into the measurement

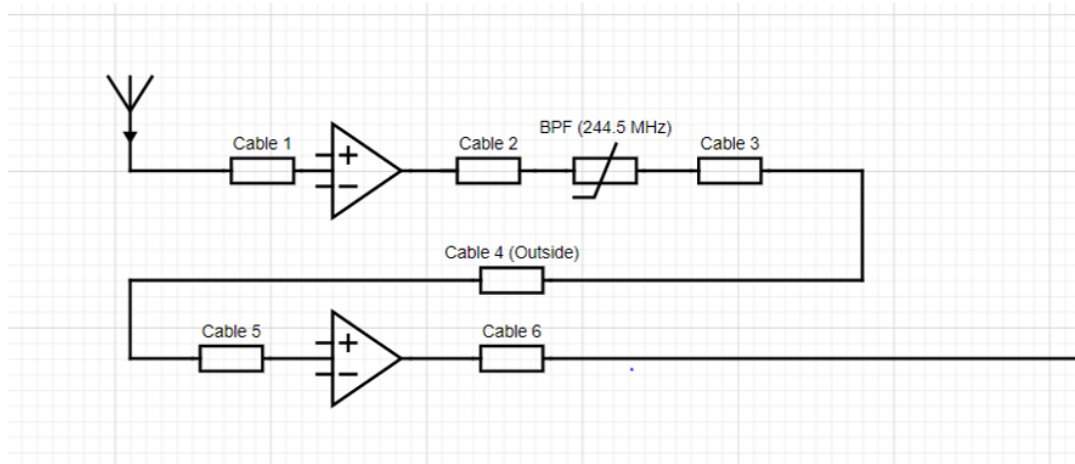


Figure 2.11: Diagram of the system layout.

device. Looking at Figure 2.11 and table 2.1 shows the layout of the system along

Table 2.1: Loss due to active components based on frequencies at 240, 244.5, and 250 MHz.

Component	240 MHz (dB)	244.5 MHz (dB)	250 MHz (dB)
LNA 1	-32.79	-32.88	- 32.32
LNA 2	-32.03	-32.16	-32.32
BPF	9.25	4.43	14.74

with the contributed by each active analog components. The calculation of the noise figure of this system can be viewed in [7]. Here it can be seen that the LNAs have a negative loss at each frequency, this is due to that they actually supply a gain of between 32.0-32.88 dB in order to compensate for approximately 2.2 dB of loss. Appendix A has the has images from of the specs for the LNAs. However, the band-pass filter does not compensate for it's loss. Its loss ranging from 9.25-14.74 dB, with the latter being at 250 MHz, but not having a precise measurement for 243.7 MHz. Here it can be inferred that at this frequency the loss lies between 4.43 and 9.25 dB. Cable losses are taken into account as well, and can be inferred further upon using [7], having a maximum loss of 0.14 dB. However, the cable used in the outside environment is had a loss of of 4.2 dB. Believed to be caused from it's worn condition. It is noted that there needs to be some slack in the cable to minimize this loss. Using **Friis' Formula** the noise factor is calculated we it is determined that the overall system noise factor is 4.37 dB. This being calculated at

the center frequency of the band-pass filter (244.5 MHz).

$$NF = F_1 + \frac{F_2 - 1}{G_1} + \frac{F_3 - 1}{G_1 G_2} + \dots + \frac{F_n - 1}{G_1 G_2 \dots G_{n-1}} \quad (2.11)$$

$$NF = 4.2 + \frac{2.2 - 1}{32.88} + \frac{4.43 - 1}{(32.88)(32.16)} + \frac{0.13 - 1}{(32.88)(32.16)} = 4.37 \text{ dB} \quad (2.12)$$

The system overall functions efficiently. However, the cable in the elements should be replaced. The analysis conducted prior calculated the noise factor being 2.005 dB at 244.5 MHz [7]. This may be due to the difference in the system setup. Where the cable with the loss of 4.2 dB is used to connect the box to the power meter, so it is not the first loss in the cascading system. This is because initial tests were done where the LNAs, band-pass filter, and batteries were all left near the radio telescope sealed in a weather proof box. For the most recent tests this box is placed inside whereas, the lossy cable is connected directly to the antenna's feed/receiving coaxial cable. Thus making it the component to characterize the over loss in the system.

CHAPTER 3

MEASUREMENTS AND DATA COLLECTION/ANALYSIS

3.1 Measurements Overview

earth Once the system was designed and tested, proper data is collected. The first tests are done by Nick Rooney, two years prior to that of the most recent results. Designing the system to operate at 250 MHz. He took tests over various lengths of time varying from 24-72 hour periods. This same approach is also taken at 243.7 MHz, for the reasons discussed in chapter 2. For the data collected at 243.7 MHz using the **DATAQ**, a sample is recorded ever 15 seconds in order to reduce the data's file size, it should be noted that this did not take away from the data integrity. The results from all of the tests are not shown, replication proved to be achievable in all instances. There were discrepancies in that the beginning and ending of the testing times were not consistent. However, the time stamps were recorded by the data acquisition device.

3.2 Preliminary Data

Although Dr. Jansky laid the ground work for this study, it replicated with radio-telescope constructed in chapter 2. Another study is that of Dr. Harry

Lenzing, who actually provided insight into the project. In doing so he provided knowledge in the detecting of galactic noise, along with proper noise temperature calculations. Dr. Lenzing and two of his former students conducted a project at Stevens Institute of Technology, where they conducted a study to verify the findings of Dr. Jansky, and others that have observed galactic noise. One student Matt Conrad built a radio-telescope in order for the measurements for the study to take place. The measurements taken showed that the only loss component of the link budget calculations is the galactic noise. With various studies having galactic noise's minimum ranging from 25 K to 34 K and its maximum from 270 k to 1000 K. Upon completion of the measurements in this study, and the use of the simulation software. It is inferred that these measurements for the various studies differ in that their locations, and times may be why the range for the maximums vary so much, as well as the system design. There is a possibility of change in the noise level through the frequency spectrum.

Nick Rooney's study is used as baseline being that this project is stimulated from the work conducted by him. Figure 3.1 shows the results from his measurements. It concurs with that shown by Dr. Jansky. It can be seen that the noise floor rises at a constant rate until it reaches a peak around midnight. The main difference between the two studies is that, from the Rooney study it cannot be determined whether or not there are multiple peaks. Unlike Dr. Jansky's studies where there are two peaks one being significantly higher than the other.

3.3 Measured Data

Once the background of what was being sought after, tests for the current project were conducted in order to establish a more detailed baseline. With the most prominent data from the previous studies being from Dr. Jansky's 24 hour tests and Nick's 48 hour, it seemed that a 72 two hour period needed be observed this being due to the Earth's rotation period actually being measured in **Sidereal Time** making a day 23 hours and 56 minutes, instead of the widely accepted 24 hours. This means the cyclic nature of galactic noise cannot only be graphed, but this graph shift by four minutes each data. Meaning that each point is measured four minutes earlier each day. Figure 3.2 shows the data collected between 3 pm on August 6 through 4 pm on August 9. It is here where it can be seen that the

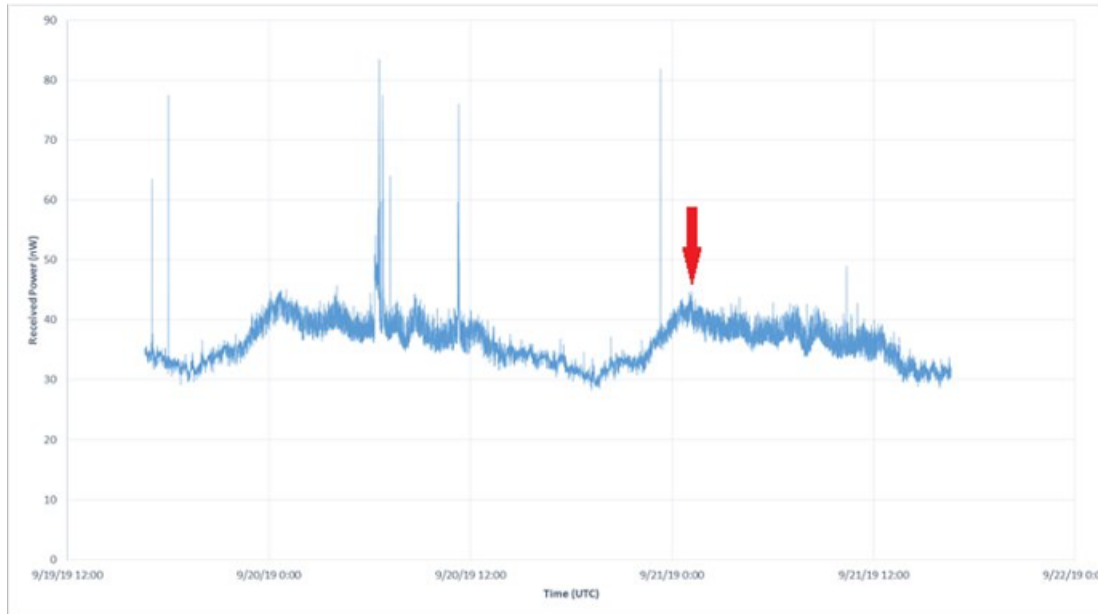


Figure 3.1: 48-hour data recorded by Nick Rooney. It can be seen that there is a pattern reoccurring, at a similar time of each day. Thus giving a cyclic nature to the data.

noise floor of the sky is not constant. As the day goes on it can be seen that the noise floor changes it rises, and falls with there being two noticeable peaks daily. Looking at the samples there are a total of 17,292 samples, whereas stated before each is recorded approximately every 15 seconds. Although the time of day would be ideal for the mapping of this shift in the noise floor. It is decided that for later comparison of the peaks, it is best to leave the sample points rather than the time stamps. This plot shows really good curves, however it seems that the smaller maximum is taking place at the beginning of the data collection process. It is later confirmed when the individual days are plotted congruently. It must be noted that although the recording of the data began during the smaller daily peak it does not end in the middle of it. Being that this data was not the first conducted during the study, an idea of the peak values had been developed, and decided it was best to let the test run beyond the 72 hour mark.

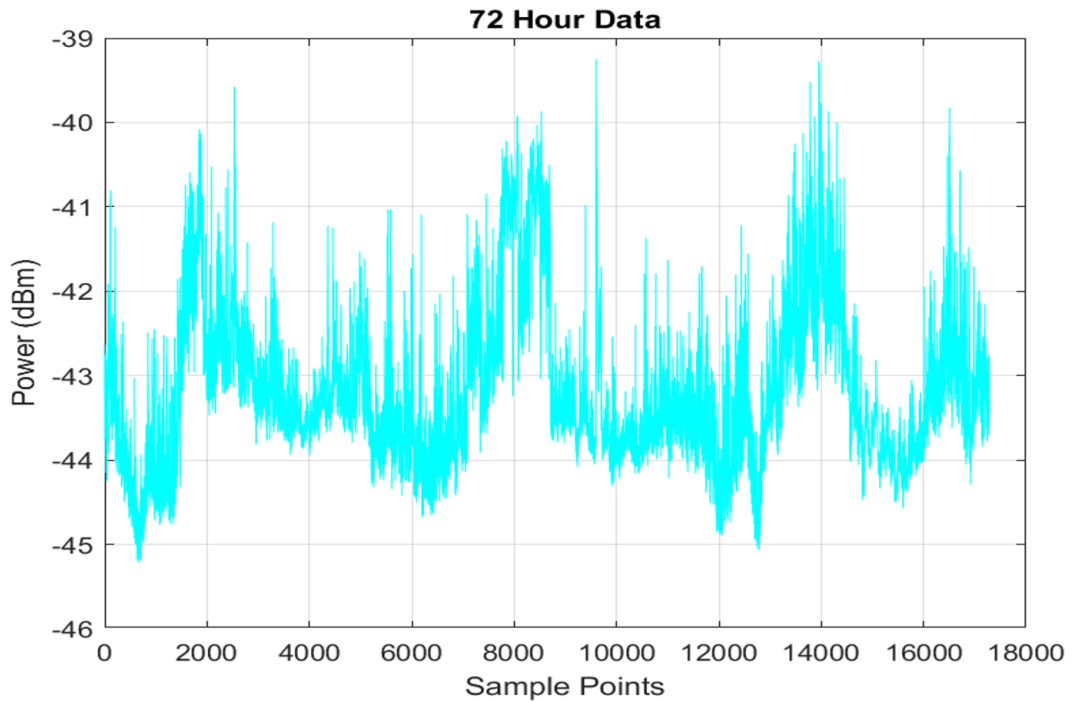


Figure 3.2: 72-hour data collection of the sky’s noise floor. The cyclic nature of galactic noise is prevalent in that the noise floor rises and falls throughout the day.

3.3.1 Daily Comparison

Using the same plot, the data is broken up into its three individual days, and plotted in congruence with one another. When this is done it can be seen that the rise in the noise floor does in fact occur around the same time daily. This can be seen in Figure 3.3, where red, blue, and green plots, represent August 6, 7, and 8 respectively. Each day being the beginning of a 24 hour cycle. Just as expected the sample points lie within the same range of one another, with slight discrepancies. This is done by dividing the three plots into three sections using the sample points. Here it can then be plotted simultaneously, helping to better see if the curves match one another. This is very important, however for the blue and green curves there should be a shift towards the left indicating an earlier changing in the noise floor, being that the time was recorded using the **meridiem** (24 hour) form of measurement, versus using the sidereal approach. This is hard to see with there being such a large sample size. In order to best test this theory the data should be collected throughout the year, and compared with one another. This is expected

for future studies, whereas these studies should not only provide a validation for the shift in the time axis, but the noise floor level as well. Being that the Earth tilts, it should be seen whether or not the sun plays a pivotal role in the noise floor level whether the Earth tilts away (fall/winter), or towards it (spring/summer). This would help further comprise the dynamic of the proposed link budget analysis. However there is but a small sample size, given that a learning curve was needed in order to fully grasp the research at hand. Other daily values were recorded, but the early results proved to be faulty. Problems with the conversion from the power meter to the DATAQ seemed to be off when first recording however the curve pattern proved to be the same. Also it must be mentioned that Nick's graphs although similar, has slight discrepancies, due to the time of year it was recorded and the sampling rate of the recording.

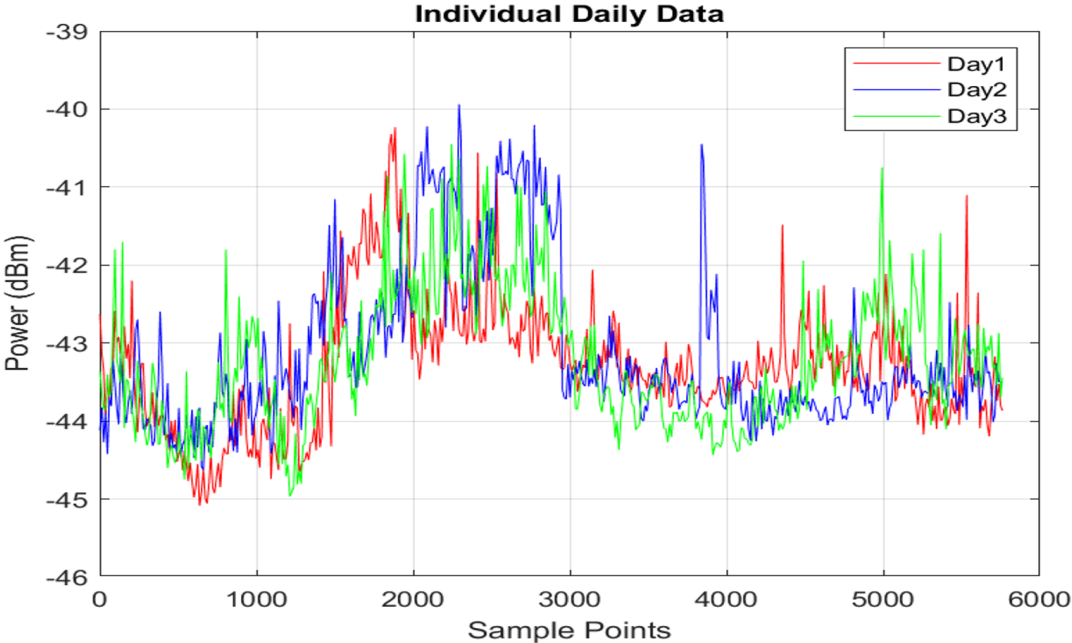


Figure 3.3: 72-hour data collection broken up into individual days, and plotted in congruent with one another.

3.4 Data Interpretation

Looking at this data it can be seen that a cyclic nature does occur. Thus implying that this is a recurring phenomena. Which insinuates future occurrences

can prudently be estimated. First it can be seen that the maximum lies from -41 and -40 dBm. Meanwhile, the second lies from -43 and -42 dBm. With the lowest minimum reaching as low as -45 dBm. Looking closely at the graph there it is clear that between the largest maxima and the local maxima the noise level does not diminish to its lowest level. This was predicted that the largest maxima is when the center of the galactic plane is within the boresight of the radio-telescope, and the second when some other part is within view. Slowly but surely it is moving out of direct view causing the noise floor to go down. That is until, the antipodal of the plane comes into direct view thus raising the noise floor higher, but not as high as the viewing of Sagittarius A. Confirmation of this is achieved through the use of the simulation software, explored in chapter 4.

CHAPTER 4

SOFTWARE IMPLEMENTATION

Although hardware implementation plays a crucial role in the experimentation process, software is just as important if not more. However, there are always physical factors that must be taken into account that isn't always accounted for in simulation. Here in this chapter an explanation is of the software and how it is used is explored. With the vast increase in knowledge of the setup of the universe, various models have been proposed, and used in interstellar simulation. It must be noted that an ideal software to use is **Systems Tool Kit (STK)**, a simulation software that helps in the modelling of orbital vehicle propagation. through the use of STK various celestial bodies can be simulated, and used to design link budgets for satellite communication systems. The first idea was to use this system to model the galactic plane and use and place a receiver on the surface of the Earth, and used the **Line-of-Sight (LoS)**, to determine when the galactic plane is in the main lobe of the aperture. Having some use to this system it could be done, thus it is proposed for a later model.

4.1 Stellarium

Stellarium is a popular free open source software used to view various celestial bodies one from another. Using this the time a viewing from a reference location such as Earth is used. For study purposes the antenna's latitude and longitude

is used to simulate when the galactic plane would come into the antenna's bore sight. In doing so the antenna's coordinates are determined using GPS, having a latitude and longitude of 40.708277° and -77.970204° . Figure 4.1 shows a picture of a part of the simulation. This image is captured at the simulation time of 1:24 am. Here it can be seen that the part of the galactic plane close to the galactic center is towards the center of the image. Here it can be seen that it is not directly over the zenith of the radio-telescope, however this should suffice in affecting any signal being received by the aperture. Although great for determining when the galactic noise should be at it's greatest, it does not show when it will begin to effect the noise floor of the system. For that Figure 4.2 is shown where in the top left of

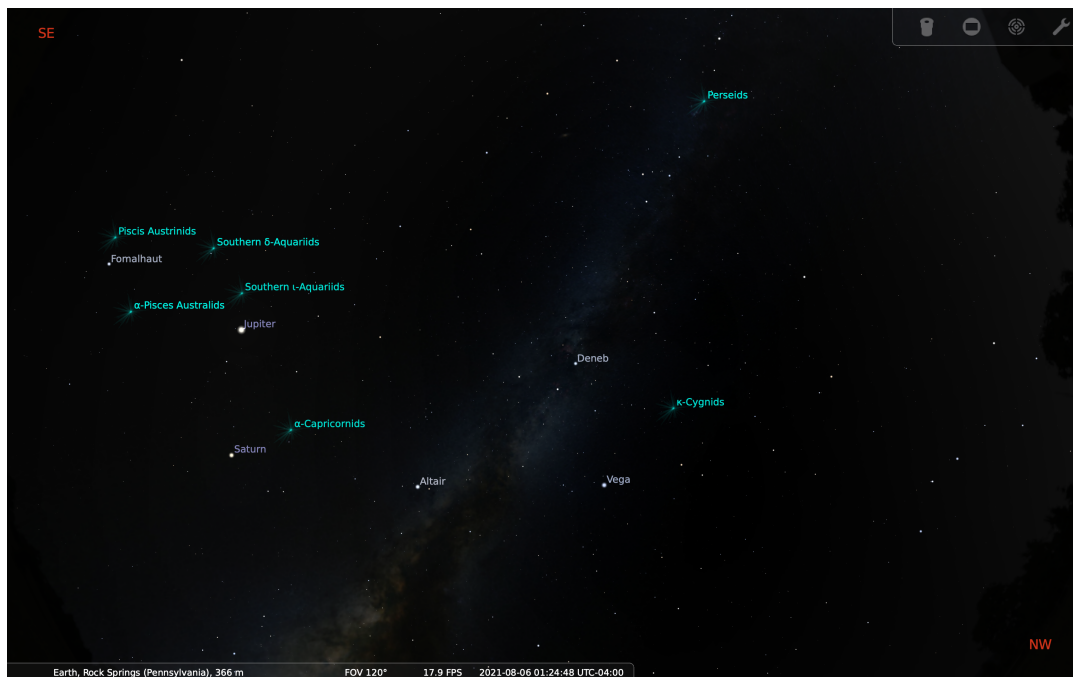


Figure 4.1: Antenna bore sight simulated using Stellarium program. Simulation time 1:24 am on Aug. 6 2021.

the image the center of the galactic plane is shown to just be entering the bore sight of the antenna. In doing so it can be seen that the galactic plane became a factor the evening before, with the date and time being Aug 5, 2021 at 6:12 pm. [h] The lower left of Figure 3.3 shows the galactic center leaving the bore sight of the antenna on Aug. 6 at 5:05 am. Meaning that the noise has been measured and collected for 13 hours. However, this is not the end of the cycle, that's because it can be seen, that the galactic plane itself remains in the view of the antenna, but a



Figure 4.2: Stellarium simulation of the galactic plane entering into the bore sight of the radio-telescope. This part of the simulation being captured at 6:12 pm on Aug. 5, 2021.

different portion of it. Causing the noise floor to once again lower, but not quite as low as, when plane is not within the aperture's bore sight. This finding is to be expected as it can be shown in the graphs that once the highest maxima of the noise floor is reached, approximately 40 dBm, the curve does not progress to it's lowest minima of approximately -45 dBm, but to roughly 44 dBm.

4.2 Simulation and Measured Data Correlation

The Stellarium simulations are used to confirm the that the readings are correct, and thus form the correlation between the galactic plane viewings and the measured data. To determine this correlation between the noise measured, and the simulation of the antenna's bore sight, Figure 4.4 is simulated. Referring back to Figure 3.2, with the start time being approximately 3:30 pm, it can be inferred that the lower maxima part of the cycle was being completed. Thus meaning that the galactic plane should be moving from out of the bore sight completely. It must be noted that that this portion of the galactic plane it hard to distinguish, glowing faintly



Figure 4.3: Galactic center leaving the bore sight of the radio-telescope. This image is simulated for the date of Aug. 6, 2021 at 5:05 am.

light blue in the bottom right portion of the Figure. However, this does confirm that what is being measured in chapter 3 is galactic noise. The next confirmation needed is the time frame of the viewing. It can be seen that from the radio-telescope measurements in Figure 3.3 that around (exact data point number)

4.3 Software Defined Radio

Another software based technology looked into is that pertaining to the replacement of the tradition radio front-end setup. This is achieved through the use of a **Software-Defined Radio (SDR)**, where both amplification, and filtering is achieved via software. In doing so, a filters bandwidth can be chosen and changed according to the designed aperture, no longer making it necessary for a physical change of the filter, however each SDR have their own max bandwidth for filtering. Another, essential piece for SDR implementation it the it's **Graph User Interface (GUI)**, where the controlling of the SDR is done along with the viewing/processing of the its transmitted data.

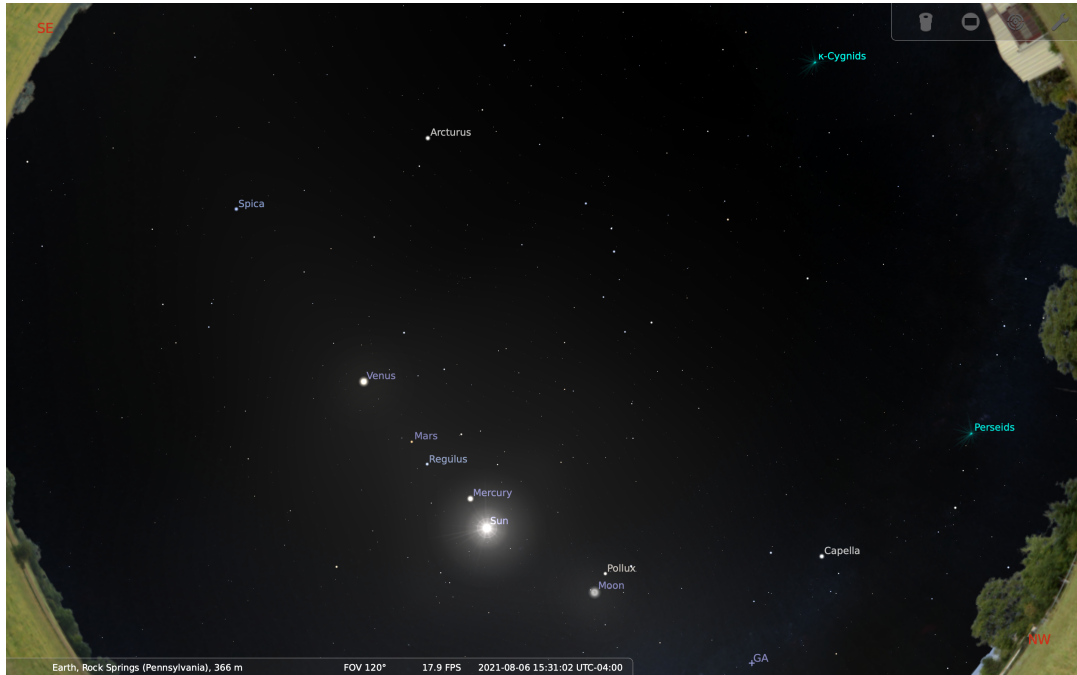


Figure 4.4: Simulation of the galactic plane exiting the bore sight of the radio-telescope. Simulated for Aug. 6, 2021 at 3:30 pm.

4.3.1 HackRF One

The chosen SDR is the **HackRF One**, shown in figure 4.5. As stated before there no longer is a need for external filtering/amplification. Thus making this device versatile in that it helps cut down on the intrinsic noise of the system. However adding its own insertion noise loss, although compensated for by its gain. Here the maximum filter width is 20 MHz, meaning that a sampling rate of 20 MHz can be used. Using a center frequency allows a range of frequencies from 234 to 254 MHz to be used. Ideally using the **Fast Fourier Transform (FFT)** would help in determining if there is any discrepancy of power throughout this smaller spectrum. This all is controller using the **GNU Radio GUI**

4.3.2 GNU Radio Companion

Control of the HackRF One is done via an open source software platform called **GNU Radio Companion(GRC)**. This GUI is python based, where flow graphs are constructed and used to interpret the data being received from the SDR. A



Figure 4.5: The HackRF One SDR. Very versatile with a half-plex setup. Used to filter and measure the signal collected by the radio-telescope.

diagram of the graph is shown in figure 4.6. Where each block serves a specific function, these are as follows:

- OSM OCOM Source
 - Used to relay the signal being measured by the HackRF.
- Fast-Fourier Transform
 - Used to see the total power being collected over the 20 MHz spectrum (234-254 MHz)
- Complex to Mag
 - Converts the received complex signal to its magnitude.
- Log10
 - Converts the linear signal into decibels.
- Vector to Stream
 - Takes the vectors and converts them into a stream data type.
- QT GUI Time Sink
 - Used to view the streamed data in the time domain.

This is how it was done when viewing the data in real time. However, with the tests being for a minimum of twenty-four hours this is not optimal, so a **Raspberry Pi** is used to run the test while away. This is done using a python script. Not only did this setup allow for a more improved data collection and interpretation,

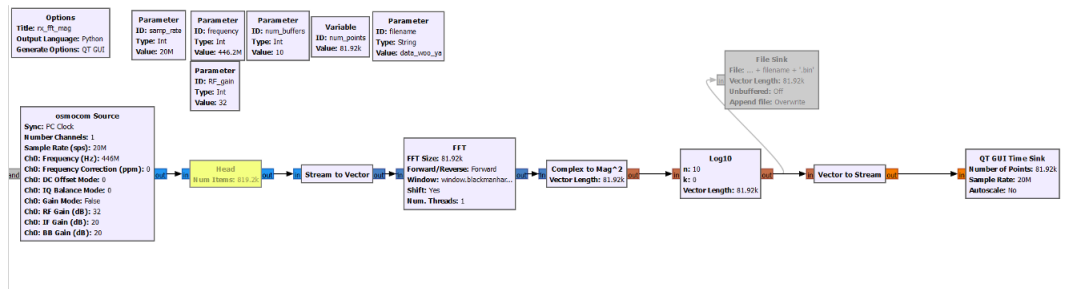


Figure 4.6: GNU Radio Companion flow graph used for the processing of the signal being collected from the radio antenna.

but it helped eliminated the use of batteries. Now the system could be powered through grid use. The results of this comes from the latest phase of testing, and has problems in the conversion, so it is not displayed in the text. However, the graphs produced it very similar to those seen in chapter 3.

4.4 WinDag

Section 2.7.2 elaborates on the DATAQ (Data Acquisition device), and how it is used in the process for the traditional RF setup. In order to run this system, the **WinDag** software is needed. It has both recording, and playback capabilities, however it is only used for the prior. These measurements can be saved in the WinDag software, or exported to and saved to and excel file for more versatile usage.

4.5 Matlab

Matlab is used for all of the data' visualization and interpretation. All graphs both seen in this thesis and unseen are produced using this language. However, with it's machine learning and pattern recognition capabilities, it is used for further evaluation. With the goal being to be able to not only map the cyclic nature, but to be able to determine the it for each unique location on Earth this proves to be very useful. Chapter 5 looks further into how this can be achieved using Matlab, elaborating on the functions used, in the hope of creating a function that can do it based on time and location.

CHAPTER 5

RESULTS/LINK BUDGET ANALYSIS

5.1 Data Analysis

Upon completion of the collected data, and that of the simulations, it can be seen the noise floor does indeed change cyclically on a daily basis. With this cycle being driven by the galactic plane, more so its center. With every cycle a plot can be applied to characterize the nature of this occurrence. For this reason it is believed that this problem can be solved using a linear regression approach. Where a line is derived to connect all of the measured data points. However, it is better to take a curve fitting approach in order to fit to data collected. Where from the multiple minimums and maximums it can be determined that there will be a polynomial to represent the curve. This curve using coefficients to help determine model makeup. Thus allowing for later use, to achieve this Matlab is used.

5.2 Curve Fitting

In order to have an idea of how to properly compensate for galactic noise, the cycle of its occurrence is first observed and recorded. Sampling every 15 seconds allows for a plot that is not overly populated, thus helping in a more distinct curve. Matlab provides two ways to use curve fitting. The first is the curve fitting tool where various types of curve fits are used to match the measured data. These fits

are the following:

- Gaussian
 - Best used for independent functions, that utilizes random variables.
- Exponential
- Polynomial
 - Used to fit data that resembles a polynomial curve.
- Linear
 - Ideally a straight line used to fit data.
- Fourier
 - Curve fitting for frequency analysis problems.
- Rational
 - Fractional setup where the function is realized through the use of the degrees in numerator and denominator.
- Sum of Sine
 - Used to fit periodic functions.
- Weibull
 - Used to analyze the life span of a product, mainly for commercial use.
- Interpolant
 - Used to connect discrete data points. Matlab had already done this through the plotting of the data.
- Smoothing Spline
 - Can be used to further smooth out a curve.

As mentioned the first idea was to use a polynomial curve. This proved to be fit well with the proposed problem. Once this tool became of familiar usage, the next approach is to determine the degree of degree of change. Instead of loading the data in the Matlab curve fitting app, it could be seen that Matlab's second approach to curve fitting can be used. This involves using the `fit()`. This function takes the same variables being plotted against one another, along with a specified type of curve it is desired to be fitted to. The first idea is that the curve has two minima and two maxima, meaning there are four degree changes, therefore a four degree polynomial should suffice. However this not the case be the magnitude of the degrees are not quite the same as can be seen in figure 5.1 (ARL Laptop). Using a degree of 5 however increased the accuracy of the curve. Further increase of the accuracy of the curve is achieved, however this comes at the cost of **over-fitting**. Over-fitting occurs when the model has been fitted to perfectly that it even recognizes any variance in trained data, that it characterizes it as a normality. In this case it would be the outliers that cause the noise levels to be higher than than those in the noticeable range. It is for this reason that the 'poly5' option is used for the `fit()` function.

5.3 Curve Fitting Results

Both the curve fitting tool and the `fit()` function were used on the seventy-two hour data set first. However, this curve proved to have a degree of difficulty, in the curve fitting process. This being the variability in the degrees of the data set. Where a typical day has four degrees of change, this set has twelve. Ideally 13 degrees are needed to properly fit the curve, but Matlab only allows up to 9 degrees. This did somewhat fit the curve, and is shown in figure 5.2, however the results are not satisfactory. The single day curves do have similarities to one another like the curves however the data may need to be averaged to get a consensus model to use for link budget calculations. Figures 5.3-5.5 show the results of each individual day through the use of the `fit()` function. The coefficients for each curve is saved to fit-object variable. With the correlation curves it can be seen that the minima and maxima values are not achieved during the 5 degree curve fitting. However, when developing the dynamics of the link budget, two options are proposed, the addition of degrees to the polynomial, or adjusting the coefficients. With the latter being

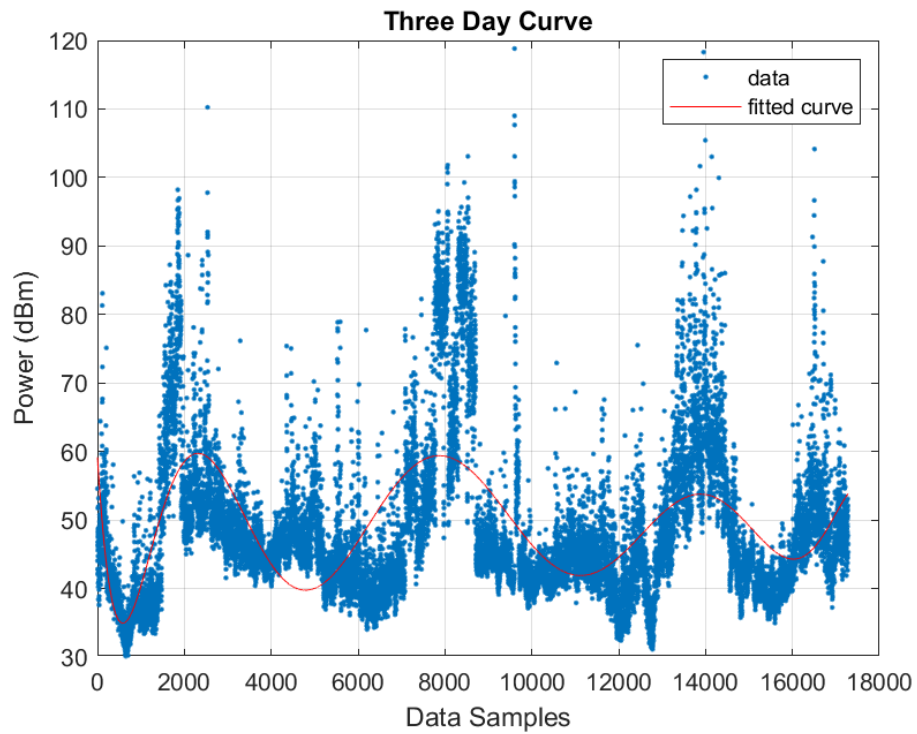


Figure 5.1: Curve fitting (9 degree polynomial) using the 72 hour data. The established curve is adapting to the data set however, it is not ideal for adaptation for future utilization.

chosen.

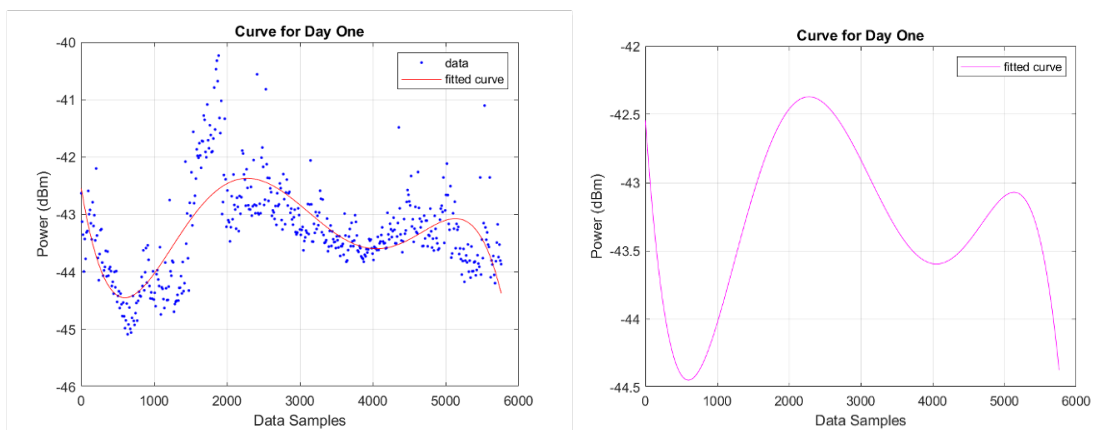


Figure 5.2: Day one five-degree curve fitted model.

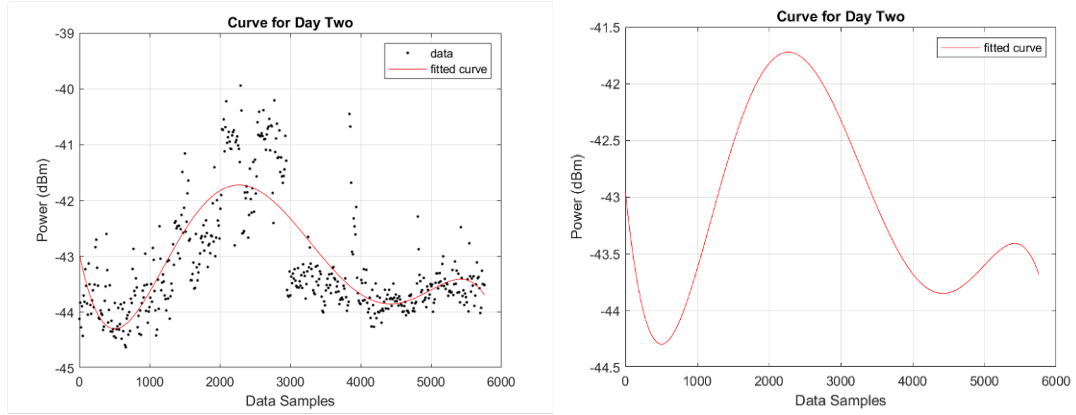


Figure 5.3: Day two five-degree curve fitted model.

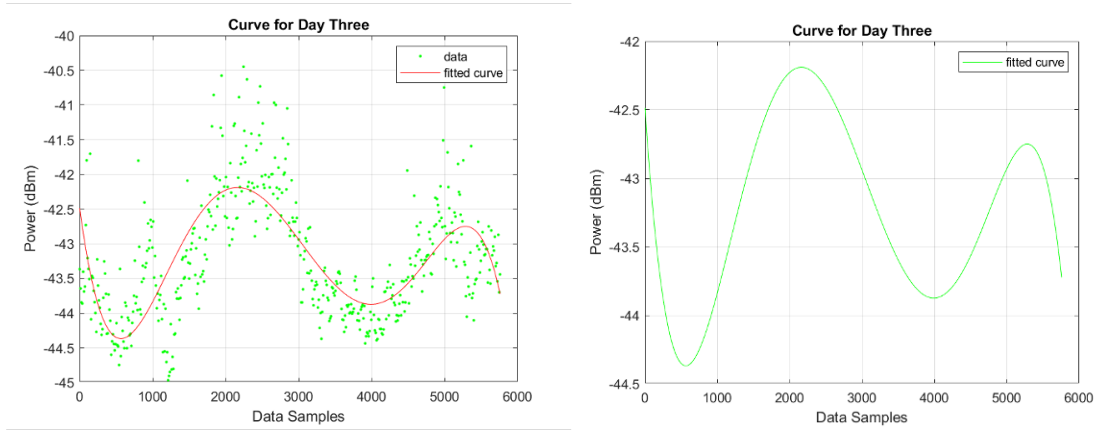


Figure 5.4: Day three five-degree curve fitted model.

5.4 Link Budget Analysis

With the goal of this study being to determine to come up with a dynamic link budget based off the cyclic nature of galactic noise, a conversion from micro-decibels to Kelvins is necessary. Where Kelvins represents the noise temperature. Neglecting all forms of loss besides that produced by the system and galactic noise. Equations 5.1-5.3 show the calculations for the system noise temperature, and the maximum difference between the minimum noise floor and maximum noise floor (using Dr. Karl Jansky's expected value of -48 dBm), roughly 8 dB. Evidently this number does change throughout the day, as can be seen on all of the produced plots.

$$K = T_{REF} \times \left(10^{\frac{NF(dB)}{10}} - 1\right) \quad (5.1)$$

$$K_{RX} = 290 \times (10^{\frac{4.37}{10}} - 1) = 466 \text{ K} \quad (5.2)$$

$$K_{GNmax} = 290 \times (10^{\frac{8}{10}} - 1) = 1540 \text{ K} \quad (5.3)$$

Where T_{REF} is the reference noise temperature of the aperture, 290 K is a widely used number. K_{RX} is the noise temperature of the system, and K_{GN} is the galactic noise. It can be seen that 2006 K ought to be added to the link budget for the a system under similar conditions, just based of the noise temperature, and maximum galactic noise alone. However, that is the worst case scenario, when the galactic noise is at its maximum.

5.5 Dynamic Link Budget

In order to not just use one figure of merit for the link budget, a dynamic link budget is proposed. In order to accomplish this a function in Matlab is being designed that uses coefficients found during the curve fitting process. In order to do so a model of the globe is simulated in Matlab with a great circle projected onto it at 63° , to represent the galactic plane. Once this is done the `antipode()` and `track()` functions is used to produce the coordinates along the plane. In doing so every location within these coordinates is being effected by galactic noise, and thus saved to an array. However, the part of the galactic plane being viewed is not the same all throughout the coordinates. Some may be looking at the galactic center meanwhile others at another part of the plane. Another consideration is the rotation of the Earth. Being that the curves produced are used for only one location, consideration of what parts of the curves based on time and location need to be taken into account for other locations. It is believed the latitude of the location plays a the significant role in determining the portion of the code used at a given point in time. Currently this phase is currently being conducted. With the hopes that it will be completed soon.

CHAPTER 6

CONCLUSION/FUTURE WORK

With the research that has been conducted, it can be seen that the noise floor does change throughout the day between 233-253 MHz. With a theoretical sky noise floor of -48 dBm, a variation from approximately -45 dBm to -40 dBm is seen. These changes are not brief, thus meaning that it should be seriously taken into account when setting up a satellite communication link, in order to ensure successful communication at all times. Improvements to the system is suggested in that cables are operating efficiently in the shielding of outside noise, in addition to the transferring of data. Along with upgrades for the LNAs and the band-pass filter. A log periodic antenna would help increase the band-width of the entire system. It is propose that future measurements be conducted with the HackRf, in doing so the entire spectrum measured by the log periodic antenna can be observed, and recorded.

6.1 Future Work

As mentioned before they is yet more work to be conducted for the completion of this project. To come up with a model for practical use more testing, must be conducted along with improvements to the system. With devices such as SDRs it is possible to increase the efficiency of data collection process, by simplifying the system setup with the addition of flexibility to the entire system.

6.1.1 Function Completion

Besides the system measurements, what is left is to take the already collected data, along with the analysis, and complete the `noise()` function to effectively produce a link budget analysis. It is believed that this is not too far from completion, but the right approach needs to be taken for an accurate model to be produced. Matlab is the language of choice, however for ease of implementation, along with speed, other languages are to be considered. Python for direct implementation through the use of GNU Radio Companion. Although limited control over the HackRf's front amplifier is given, it is possible to use one of the HDL languages for control of such features/function implementation, as well as an increase in speed these being:

- VHDL
- Verilog
- System Verilog

6.1.2 System Components

As for the system measurements it has been noted that it must be taken into consideration that the LNAs operate optimally at 25° C. The first tests were conducted with the RF setup outside in the elements. However, as the for the calculations and the measurements presented in this thesis the RF components stayed inside a storage bin, where the temperatures outside exceeded 32° C. The effects need to be further studied in order to determine the complete accuracy of the calculations. Appendix A shows that as the temperature rises causing a decrease in the gain due to an increase in the insertion loss. It is proposed to do away with bandpass filter, where the HackRF is used instead for the filtering process, and along with the elimination of the LNAs. As well as the cables connecting them. Helping to lower the noise factor to that of a cable with a lower insertion loss. With the HackRF there is no longer a need for the power meter nor the data acquisition device. Meanwhile, the capability to determine the noise power over a wider frequency spectrum. Thus determining whether or not the noise characteristics' consistency throughout the spectrum. This can be taken simultaneously while the `noise()` function is fine tuned.

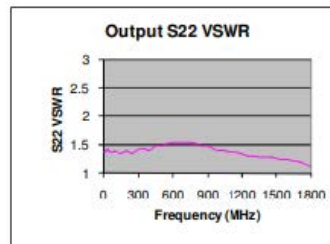
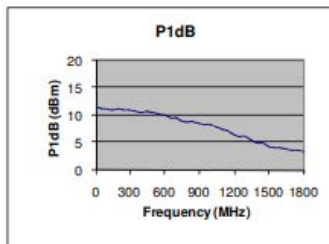
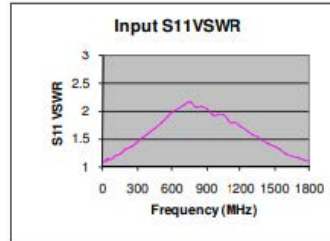
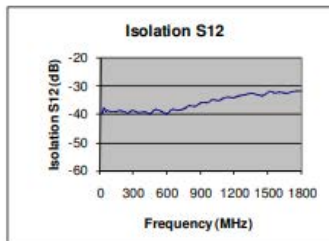
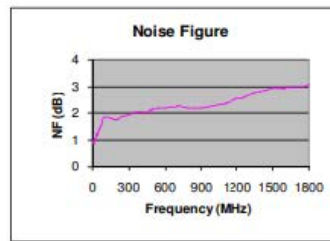
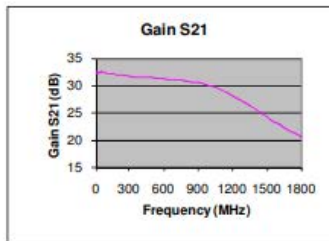
6.2 Conclusion

Suggested improvements leaves much to be desired for this project. In doing so many applications can be added in order to improve the system operation. With the first step being to finish the function, and its fine tuning through the use of component improvements. However, the numbers will not be exact, but this thesis does indeed imply that galactic noise is a problem of time and place. Meaning it needs to be compensated for, but not over compensated.

APPENDIX A

LOW NOISE AMPLIFIERS DATA SHEET

Typical Performance @ +25°C



Features

- Frequency Range:1KHz-1800MHz
- Gain: 30dB @ 1000MHz
- P_{1dB}: +8dBm
- IP3: +20dBm
- Noise Figure: 2.2dB
- Reverse Voltage Protected
- SMA Connector

Picture



Performance Measured @ 1000MHz

Description

LNA-1800 is a 30dB gain wideband Low Noise Amplifier operates with frequency range from 1KHz to 1800MHz.

Electrical Specifications @ +25°C, Z_{in} = Z_{out} = 50 Ω, Vcc = +12V

Parameter	Unit	Minimum	Typical	Maximum
Frequency Range	MHz	0.001		1800
Gain f = 1KHz	dB		30.0	
f = 50KHz	dB		31.0	
f = 500KHz	dB		32.5	
f = 10MHz	dB		32.4	
f = 100MHz	dB		32.2	
f = 1000MHz	dB		30.0	
f = 1500MHz	dB		24.0	
f = 1800MHz	dB		20.5	
P _{1dB}	dBm		+8	
IP3	dBm		+20	
Noise Figure	dB		2.2	
Reverse Isolation	dB		-35	
VSWR Input VSWR			1.9:1	
Output VSWR			1.4:1	
DC Power Supply	V	11	12	24
Supply Current	mA		40	

APPENDIX B

MATLAB CODES

```

clear;
close all;

file = readtable('Aug6_9_72hr.xlsx');
file.TimeStampUTC = datevec(file.TimeStampUTC);

display(file.TimeStampUTC(end,:));
file.TimeStampUTC = file.TimeStampUTC(:,4:6);
disp(length(file.TimeStampUTC));
num = length(file.TimeStampUTC);
time = (1:length(file.TimeStampUTC)).';

figure;
plot(time(:,1),10*log10(file.nW*1e-9)+30,'c');
grid on;
hold on;
title('72 Hour Data');
xlabel('Sample Points');
ylabel('Power (dBm)');
saveas(gcf,'72 Hour Data.png');
num1 = ceil(num/3);
num2 = ceil(2*num1);
d1 = file.nW(1:num1);
time1 = length(d1);
hold off;
figure;
plot(1:12:time1,10*log10(file.nW(1:12:num1)*1e-9)+30,'r');
hold on
plot(1:12:num1,10*log10(file.nW(num1:12:num2)*1e-9)+30,'b');
plot(1:12:num1,10*log10(file.nW(num2:12:num)*1e-9)+30,'gr');
grid on;
legend('Day1','Day2','Day3');
title('Individual Daily Data');
xlabel('Sample Points');
ylabel('Power (dBm)');
saveas(gcf,'Daily Split Data.png');

```

```

gnoise = file.nW;
pd1 = 10*log10(file.nW(1:12:num1)*1e-9)+30;
pd2 = 10*log10(file.nW(num1:12:num2)*1e-9)+30;
pd3 = 10*log10(file.nW(num2:12:num)*1e-9)+30;
d1 = (1:12:time1).';

d1curve = fit(d1,pd1,'poly5');
figure;
plot(d1curve,d1,pd1);
title('Curve for Day One');
xlabel('Data Samples');
ylabel('Power (dBm)');
grid on;
saveas(gcf,'Curving Fitting1.png');

d2curve = fit(d1,pd2,'poly5');
figure;
plot(d2curve,d1,pd2,'.k');
title('Curve for Day Two');
xlabel('Data Samples');
ylabel('Power (dBm)');
grid on;
saveas(gcf,'Curving Fitting2.png');

d3curve = fit(d1,pd3,'poly5');
figure;
plot(d3curve,d1,pd3,'.gr');
title('Curve for Day Three');
xlabel('Data Samples');
ylabel('Power (dBm)');
grid on;
saveas(gcf,'Curving Fitting3.png');

curve72 = fit(time,gnoise,'poly9');
figure;
plot(curve72,time,gnoise,'.');
title('Three Day Curve');

```

```

xlabel('Data Samples');
ylabel('Power (dBm)');
grid on;
saveas(gcf, 'Curving Fitting72.png');

figure;
plot(d1curve, 'm');
title('Curve for Day One');
xlabel('Data Samples');
ylabel('Power (dBm)');
grid on;
saveas(gcf, 'Curving1 Fitting.png');

figure;
plot(d2curve, 'r');
title('Curve for Day Two');
xlabel('Data Samples');
ylabel('Power (dBm)');
grid on;
saveas(gcf, 'Curving2 Fitting.png');

figure;
plot(d3curve, 'gr');
title('Curve for Day Three');
xlabel('Data Samples');
ylabel('Power (dBm)');
grid on;
saveas(gcf, 'Curving3 Fitting.png');

```

REFERENCES

- [1] K. Jansky, "Minimum noise levels obtained on short-wave radio receiving systems," *Proceedings of the IRE*, vol. 25, no. 12, p. 1517–1530, 1937.
- [2] —, "Electrical disturbances apparently of extraterrestrial origin," *Proceedings of the IRE*, vol. 21, no. 10, p. 1387–1398, 1933.
- [3] S. Kwok, "The plurality of worlds," *Our Place in the Universe - II*, p. 101–111, 2021.
- [4] E. P. Hubble, "Extragalactic nebulae." *The Astrophysical Journal*, vol. 64, p. 321, 1926.
- [5] Q. D. Wang and S. Stolovy, "Galaxy classification - the university of western australia," 2014. [Online]. Available: <https://www.uwa.edu.au/science/-/media/Faculties/Science/Docs/Galaxy-classification.pdf>
- [6] L. Billings, "Astronomers are finally mapping the "dark side" of the milky way," Oct 2017. [Online]. Available: <https://www.scientificamerican.com/article/astronomers-are-finally-mapping-the-dark-side-of-the-milky-way/>
- [7] W. Fletcher, *Noise Figure Analysis of Radio Telescope Receiver Chain*, May 2021.
- [8] K. Corporations, "Link budget calculations for a satellite link with an electronically steerable antenna terminal," Jun 2019. [Online]. Available: <https://www.kymetacorp.com/wp-content/uploads/2020/09/Link-Budget-Calculations-2.pdf>
- [9] B. F. Burke, "Radio radiation from the galactic nuclear region," *Annual Review of Astronomy and Astrophysics*, vol. 3, no. 1, p. 275–296, 1965.

- [10] E. Franke and G. Vaal, “Link margin for uhf airborne satellite communications (satcom) operation,” *Proceedings of the IEEE 1996 National Aerospace and Electronics Conference NAECON 1996*.
- [11] C. Allen and C. Gum, “Survey of galactic radio-noise at 200 mc/s,” *Australian Journal of Chemistry*, vol. 3, no. 2, p. 224, 1950.
- [12] J. D. Kraus, *Radio Astronomy - John Daniel Kraus ; with a chapter on radio - telescope receivers*. McGraw-Hill, 1966.
- [13] H. Lenzing, *Galactic Noise*, 2021.
- [14] A. Rudge and M. Withers, “Design of flared-horn primary feeds for parabolic reflector antennas,” *Proceedings of the Institution of Electrical Engineers*, vol. 117, no. 9, p. 1741, 1970.
- [15] K. Singh, A. V. Nirmal, and S. V. Sharma, “Link margin for wireless radio communication link,” *ICTACT Journal on Communication Technology*, vol. 8, no. 3, p. 1574–1581, 2017.
- [16] K. G. JANSKY, “Radio waves from outside the solar system,” *Nature*, vol. 132, no. 3323, p. 66–66, 1933.

[1] [2] [3] [4] [5] [6] [7] [8] [9] [10] [11] [12] [13] [14] [15] [16]

Vita
Terele Parker

EDUCATION

Tuskegee University, Tuskegee, AL, USA
B.S. Electrical Engineering, May 2020
The Pennsylvania State University, State College, PA, USA
M.S. Electrical Engineering August 2022

WORK EXPERIENCE

The Applied Research Laboratory at Penn State, State College, PA, USA
Graduate Research Assistant May 2020 - Present

ACADEMIC RESEARCH EXPERIENCE

Tuskegee University Microelectronics Laboratory, Tuskegee, AL, USA
Undergraduate Research Assistant August 2018 - May 2020
University of Tennessee Chattanooga, URACE, Chattanooga, TN, USA
Undergraduate Researcher June 2019 - August 2019
The Applied Research Laboratory at Penn State, State College, PA, USA
Intern June 2018 - August 2018